Ore Geology Reviews 146 (2022) 104932

Contents lists available at ScienceDirect

Ore Geology Reviews

journal homepage: www.elsevier.com/locate/oregeorev

A synthesis of the geology, spatial–temporal distribution and enrichment mechanism of granite-related indium deposits in China

Taiping Zhao [a,b,c,*], Cheng Chen [a,b,c], Xiaohu He [d], Lei Meng [e], Jing Xu [f], Wenyuan Liu [f]

[a] Key Laboratory of Mineralogy and Metallogeny, Guangzhou Institute of Geochemistry, Chinese Academy of Sciences, Guangzhou 510640, China
[b] CAS Center for Excellence in Deep Earth Science, Guangzhou 510640, China
[c] University of Chinese Academy of Sciences, Beijing 100049, China
[d] School of Earth Sciences, Yunnan University, Kunming 650500, China
[e] State Key Laboratory of Ore Deposit Geochemistry, Institute of Geochemistry, Chinese Academy of Sciences, Guiyang 550081, China
[f] Zijin School of Geology and Mining, Fuzhou University, Fuzhou 350108, China

ARTICLE INFO

Keywords:
Enrichment mechanism of indium in Sn-polymetallic deposits
Sn-poor polymetallic Indium deposits
Sphalerite
Magmatic-hydrothermal deposits
China

ABSTRACT

China has abundant indium resources and is the main supplier of refined indium in the world. In this contribution, we systematically summarize the geology and spatial–temporal distribution of indium deposits in China, with emphasis on the genesis and enrichment mechanism of these deposits. The indium resources in China are mainly from Sn-polymetallic deposits related to Mesozoic granites within the southern Great Xing'an Range, southwestern Yangtze Block, western Nanling Range, and their surrounding regions. Moreover, these Mesozoic granitic intrusions are mainly composed of highly fractionated S- or A-type granites with peraluminous characteristics (A/CNK > 1.1) and high volatile concentrations, which are considered to be generated by biotite-dehydration melting in the crust. Because biotite is an important carrier of tin and indium, the breakdown of biotite during partial melting could release tin and indium into magmatic-hydrothermal system, leading to Sn-In mineralization. During the precipitation of indium minerals from ore-forming fluids, it is preferentially incorporated into sphalerite lattice by a coupled substitution of $In^{3+} + Cu^{+} \leftrightarrow 2Zn^{2+}$, causing a decoupling from tin. Therefore, indium resources are dominantly sourced from sphalerite-bearing ores in Sn-polymetallic deposits in China. Recently, indium mineralization has been discovered in Sn-poor polymetallic deposits (e.g., the Qibaoshan Cu-polymetallic deposit); however, the enrichment mechanism of indium in Sn-poor deposits is still unclear. Consequently, we suggest that future studies should focus on the enrichment mechanism of indium in Sn-poor polymetallic deposits and the behavior of indium in magmatic-hydrothermal systems, which would contribute to a better understanding of the coupling and decoupling of tin and indium and their metallogenesis.

1. Introduction

Indium (In), as a silvery-white metal and was discovered in 1863 by two German chemists, Ferdinand Reich and Hieronymous Theodor Richter, from the analysis of zinc ores in the Freiberg district, Germany (Schwarz-Schampera and Herzig, 2002). Indium has two isotopes, ^{113}In and ^{115}In (accounting for 4.3% and 95.7%, respectively), and has two oxidation states of +1 and +3, with +3 as the most common valence state (Schwarz-Schampera, 2014). Because of its good ductility, plasticity, light permeability and electrical conductivity, indium is widely used in the electronics, semiconductor, and aerospace industries, thereby playing a significant role in national security and the economy (Werner et al., 2017). Since the 21st century, with the boom in information technology and the new energy industry, the global consumption of indium has increased rapidly, and indium is considered as a critical metal (Schulz et al., 2017; European Commission, 2019).

The indium contents in the upper continental crust, oceanic crust, chondrites, and seawater are approximately 0.056 ppm, 0.072 ppm, 0.08 ppm and 0.2–0.7 ppb, respectively (Schwarz-Schampera, 2014; Rudnick and Gao, 2014). It is difficult to form deposits wherein indium is the primary product. Most indium deposits are granite-related and are associated with Sn-polymetallic deposits in Bolivia, China, Japan, Russia and Canada (Ishihara et al., 2006, 2011a, 2011b; Werner et al., 2017; Xu and Li, 2018). As an important indium producer, China supplied nearly half of the global total refined indium during 2011–2021 (USGS, 2021). In China, indium deposits are granite-related, such as the cassiterite-

* Corresponding author at: 511 Kehua Street, Wushan, Tianhe District, Guangzhou GD 510640, China.
E-mail address: tpzhao@gig.ac.cn (T. Zhao).

https://doi.org/10.1016/j.oregeorev.2022.104932
Received 20 February 2022; Received in revised form 6 May 2022; Accepted 9 May 2022
Available online 12 May 2022

sulfide deposits with relatively high mineralization temperatures. Low-temperature deposits without magmatic fluid components generally contain negligible indium (Zhang, 1987, 1998; Cook et al., 2009; Ye et al., 2011). To better understand the enrichment mechanism of indium, in this contribution, we systematically summarize the latest research advances of these granite-related indium deposits in China including the geological characteristics, temporal-spatial distribution, mineralization processes, and occurrence of indium. Finally, we propose the major unresolved scientific problems about indium deposits for future studies.

2. Spatial and temporal distribution of indium deposits in China

Mainland China tectonically consists of several blocks and orogens, including the North China Block, Tarim Block, Yangtze Block, Central Asian orogen, Central China orogen, and Tibet-Sanjiang orogen (Fig. 1) (Deng et al., 2017). Most large indium deposits are related to Mesozoic granites and mainly distributed in the southern Great Xing'an Range, southwestern Yangtze Block, western Nanling Range, and their surrounding regions (Figs. 1 and 2) (Xu and Li, 2018; Li et al., 2019). In this section, the general features of eight representative In-rich deposits are summarized in Supplementary Table S1 and detailed descriptions are given as follows.

2.1. Indium deposits in the southwestern Yangtze Block

The Yangtze Block is one of the major Precambrian blocks that compose mainland China (Zhang, 2017). Numerous and diverse mineralization are extensively distributed in this block, of which the Sn-In deposits in the southwestern Yangtze Block (SYB) are the well-known providers of indium resources worldwide (Hu et al., 2020). In the SYB, several world-class Sn-In deposits, such as the Dachang, Gejiu, and Dulong deposits, have been discovered in a Devonian to Triassic rift basin (Youjiang Basin) (Fig. 3) (Wang et al., 2020). Available data show that this region contains nearly 20 kt indium (Ishihara et al., 2011a; Li et al., 2015; Xu and Li, 2018), making the SYB the most important In-rich region in China (Hu et al., 2020; Li et al., 2020).

The **Dulong Sn-Zn-In polymetallic deposit,** located in the Maguan County, Yunnan Province, is the largest In-rich skarn-type deposit in mining in China (Fig. 4a-b) (Hu et al., 2020). It contains approximately 7.0 kt In, as well as 0.40 Mt Sn, 4.0 Mt Zn, 0.20 Mt Cu, and minor Pb, Ag, and Cd (Li et al., 2016). The average grade of indium is 183 ppm, which is much greater than the minimum grades (5–10 ppm) for industrial operation (Ishihara et al., 2011a). The deposit is composed of the Huashitou, Tongjie, Manjiazhai, Laizizhai, Wukoutong, and Nandangchang ore sections from south to north (Fig. 4a). Previous geological investigations suggest that all ore bodies are hosted by the Cambrian marble and quartz mica schist and are controlled by N-S-trending faults (Fig. 4a-c) (Li et al., 2016). The ore minerals in these orebodies mainly comprise cassiterite (SnO_2), sphalerite (ZnS), magnetite (Fe_3O_4), chalcopyrite ($CuFeS_2$), pyrite (FeS_2), pyrrhotite ($Fe_{1-x}S$) and galena (PbS) (Fig. 4f-k). In this deposit, the Laojunshan granite composed of two-mica monzogranite mainly crops out in the northern part of the ore field (Fig. 4a) (Xu et al., 2015). Drilling data suggest that the Laojunshan

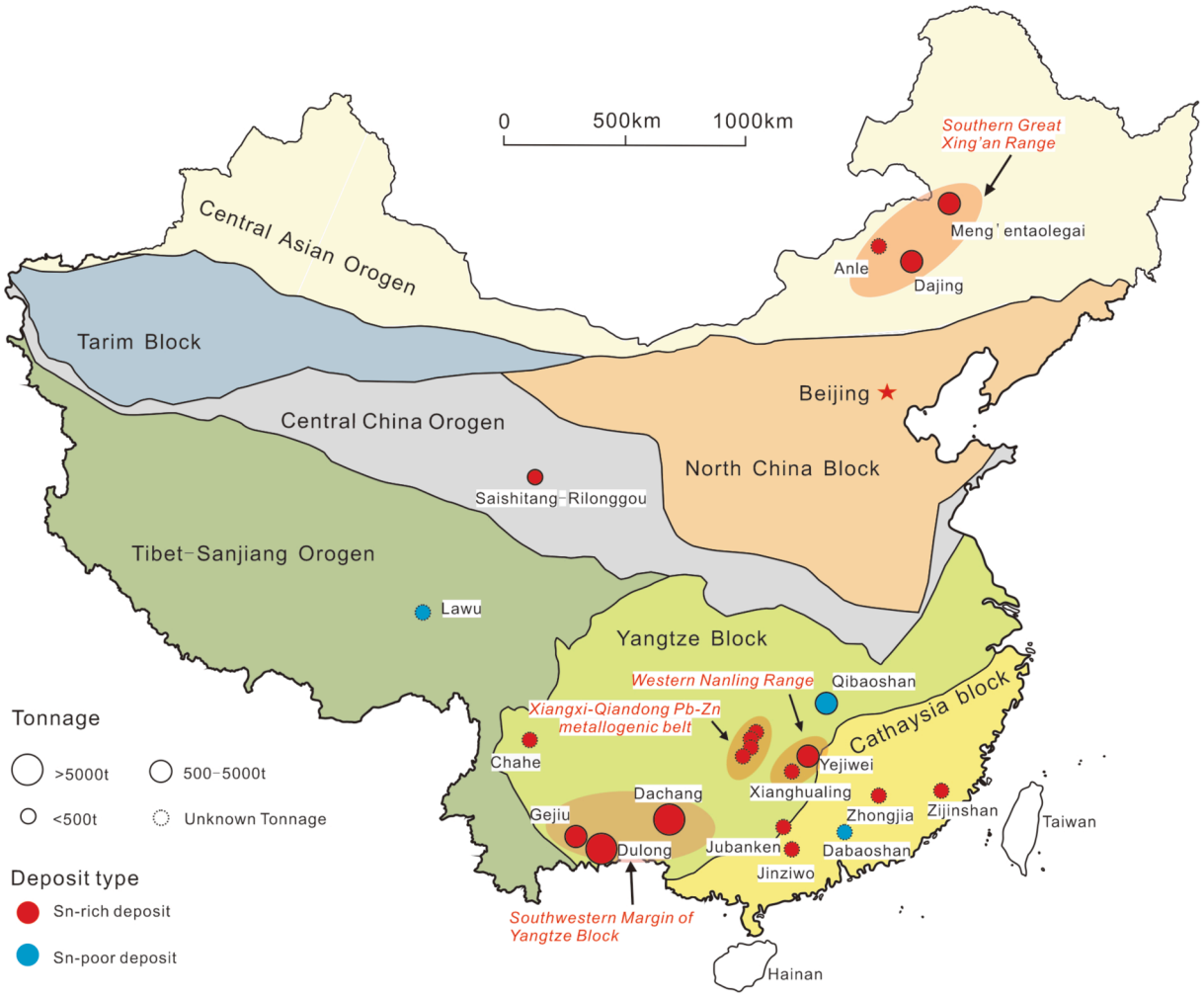

Fig. 1. Distribution of In-rich deposits in China (modified after Liu et al., 2016).

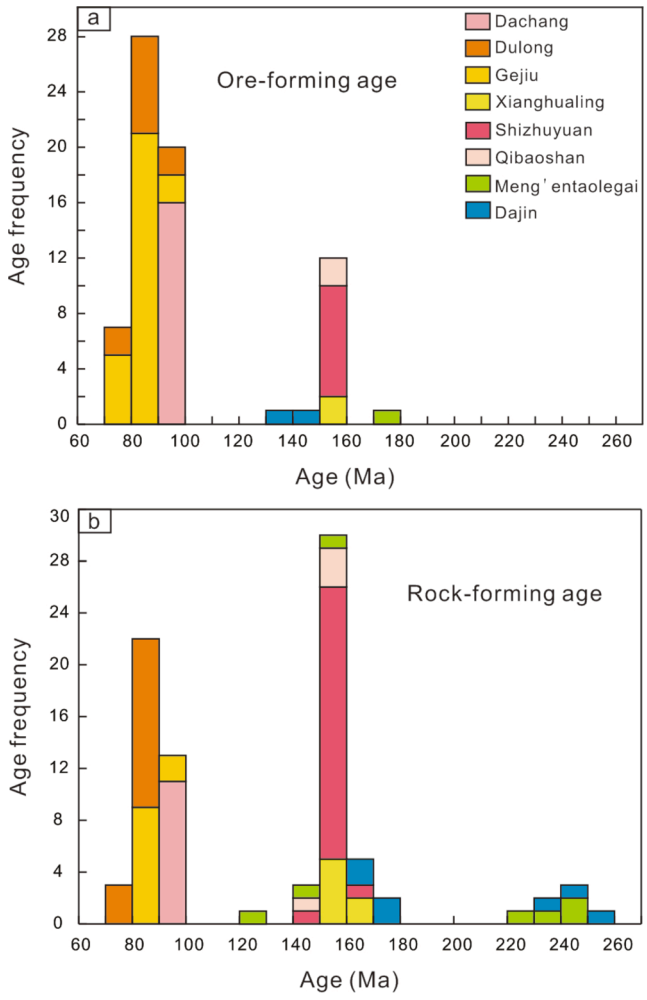

Fig. 2. Histogram of mineralization (a) and magmatism ages (b) of In-rich deposits in China. Data sources are listed in Supplementary Table S2 and S3.

granite extends southward with a dip of 15–20° and is concealed below the main ore sections (Li et al., 2016). Cassiterite U–Pb dating suggests that the mineralization occurred from 97.5 Ma to 79.8 Ma (Liu et al., 2007; Zhao et al., 2018b), which is consistent with the emplacement age of the Laojunshan S-type granite (92.9–82.8 Ma) (Xu et al., 2015). Therefore, previous studies have proposed that the Dulong Sn-polymetallic deposit is a magmatic-hydrothermal skarn-type deposit related to Mesozoic granitic magmatism (Xu et al., 2015; Zhao et al., 2018b). This viewpoint is also supported by trace element studies on sphalerite, scheelite, magnetite, pyrite, and cassiterite (Ye et al., 2017, 2018; Niu et al., 2020; Liu et al., 2021a, 2021b). According to the LA-ICP-MS (Laser Ablation Inductively Coupled Plasma Mass Spectrometry) data of sulfides from the Dulong deposit, sphalerite has 0.74 to 4572 ppm indium and is the most important host of indium (Ye et al., 2017; Xu et al., 2021a, 2021b). Recently, some sphalerite blebs, with a maximum indium concentration of ~15 wt%, were found in hornfels-hosted pyrrhotite in the Dulong deposit (Xu et al., 2021a, 2021b). Additionally, andradite from the Dulong deposit has been found to have 166 to 629 ppm indium (Xu et al., 2021b). Because it is an abundant silicate mineral in skarn-type deposits, the indium resources hosted in andradite may be considerable.

The **Dachang Sn-polymetallic deposit** is located in the Nandan County, Guangxi Province (Fig. 3). This deposit has a long mining history extending to the Song Dynasty (960 to 1279 CE) (Guo, 2019). The reserves are approximately 9.0 kt In with high average ore grade of 117 ppm (Ishihara et al., 2011a), as well as 1.5 Mt Sn, 6.8 Mt Zn, 1.4 Mt Pb, and 0.4 Mt Cu (Pi et al., 2019). The deposit comprises six ore sections: Tongpokeng-Changpo, Gaofeng, Lama, Chashan, Kangma, and Huile, where orebodies occur as layers, lenses, and veins hosted in the Middle-Upper Devonian carbonate and clastic rocks (Fig. 5a-b) (Guo, 2019). Ore minerals in these orebodies include cassiterite, sphalerite, arsenopyrite (FeAsS), pyrite, pyrrhotite, galena, and jamesonite ($Pb_4FeSb_6S_{14}$) (Guo et al., 2018b; Pi et al., 2019). In this district, the Cretaceous intrusions are widely distributed, including biotite granite (Longxianggai granite), diorite, and granite porphyry dikes (Li et al., 2010). The Longxianggai granite (96.6–90.8 Ma, Huang et al., 2019) related to mineralization is the largest intrusive body, which is considered to be a peraluminous S-type granite with high A/CNK (1.14–1.20) (Zhao et al., 2021; Huang et al., 2019). Because its cassiterite U–Pb dating yield mineralization ages ranging from 95.8 Ma to 90.3 Ma (Guo et al., 2018b), coinciding with zircon U-Pb ages of the Liangxianggai granite (96.6–90.8 Ma), tin mineralization is considered to be associated with the Late Cretaceous granitic magmatism (Guo et al., 2018b; Huang et al., 2019). In terms of ore minerals, *in-situ* analysis demonstrates that the main carrier of indium is sphalerite with an average concentration of 1020 ppm (Murakami and Ishihara, 2013). Considering that the Cretaceous granite in the ore field have higher indium concentrations (0.14–6.8 ppm) than the nearby sedimentary rocks (<0.10 ppm) (Fan et al., 2004; Li et al., 2010) and the indium content of sphalerite decreases outward from the central of intrusive body (Wu, 2009; Dai et al, 2012; Pi et al., 2015), previous studies attributed the indium mineralization to the In-rich magma produced by partial melting of In-rich protoliths in the crust (Li et al., 2010; Huang et al., 2019).

The **Gejiu Sn-polymetallic deposit**, located in Gejiu County (Fig. 5c), Yunnan Province, is the largest primary Sn-polymetallic deposit in the world (Fig. 5c) (Xu et al., 2021c). The earliest mining history dates back to the Spring and Autumn Period (770 to 476 BCE), and large-scale mining activity started in the last century (Guo, 2019). This deposit has a total reserve of ~4.0 kt In with an average grade of 207 ppm (Li et al., 2015) and contains 3.3 Mt Sn, 3.3 Mt Cu, 4.3 Mt Pb + Zn, and 0.15 Mt WO_3 (Guo, 2019). Almost all of the deposits are clustered in the western part of the Gejiu mining district, wherein six deposits were separated by E-W trending faults, including Malage, Songshujiao, Gaosong, Tangziwa, Laochang, and Kafang from north to south (Fig. 5c) (Li et al., 2015; Guo et al., 2018a). Due to the extensive hydrothermal alteration, there are six ore styles recognized: massive sulfide, Sn–granite, skarn, greisen, veined tourmaline, and stratiform-like oxidized ores (Guo, 2019). The orebodies generally occur along the contact zone between granitic rocks and Triassic carbonates (Fig. 5d) (Li et al., 2015; Xu et al., 2021c). Ore minerals in these orebodies are mainly composed of cassiterite, chalcopyrite, pyrrhotite, sphalerite, pyrite, galena, scheelite ($CaWO_4$), and wolframite ($(Fe, Mn)WO_4$) (Cheng et al., 2012; Guo et al., 2018a). Previous investigation suggested that the igneous rocks in the Gejiu mining district mainly consist of gabbro, mafic microgranular enclave-bearing granite, biotite granite, syenite, and mafic dikes (Cheng and Mao, 2010). Geochronological studies indicate that the mineralization events dominantly span from 85.6 to 76.4 Ma (Guo et al., 2018a), which agrees with the emplacement age of Late Cretaceous granitoids (85.8–77.4 Ma) (Cheng et al., 2013). Consequently, mineralization in the Gejiu district is considered to be associated with the Late Cretaceous magmatism (Cheng et al., 2012; Guo et al., 2018a). Although there are few previous reports in the literature of indium mineralization in the Gejiu Sn-polymetallic deposit, dzhalindite ($In(OH)_3$), an indium mineral formed in a hypergene environment, was found in oxidized ores in the deposit (Li et al., 2015). This result is further supported by study of Guo et al. (2020), who found that indium is highly concentrated in interlayer oxidized ores (182 ppm) but not primary sulfide ores (0.21 ppm), indicating the immobility of indium during the oxidation process. Regardless of this observation, the most economical In-bearing mineral is still sphalerite with high indium concentrations (493–4781 ppm) (Li et al., 2015).

Except for the Sn-polymetallic deposits in the SYB described above,

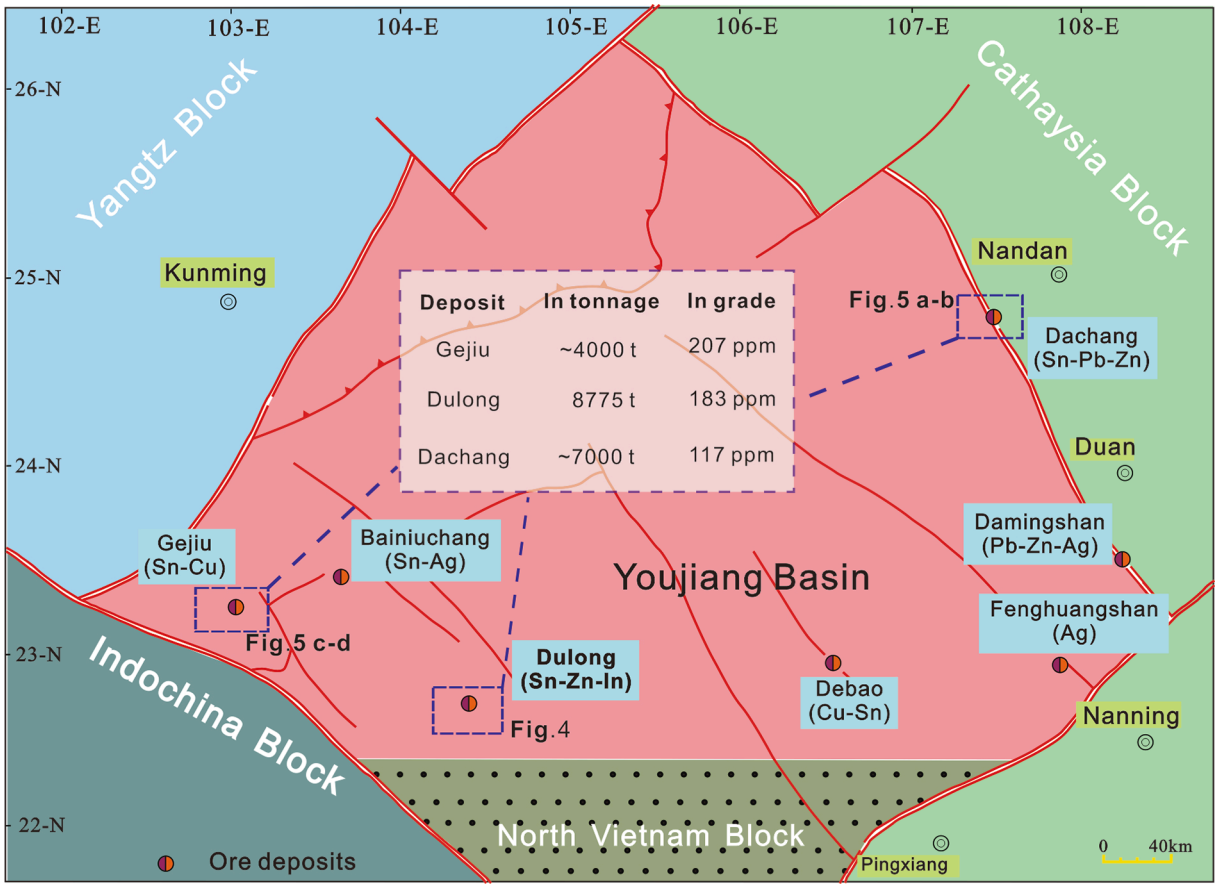

Fig. 3. Schematic map showing the distribution of major deposits in the Youjiang Basin (modified after Guo et al., 2018a). The Dulong, Dachang, and Gejiu deposits are the primary indium deposits in this region. The tonnage and grade of indium are from Ishihara et al. (2011a), Murakami and Ishihara, (2013), Li et al. (2015), and Li et al. (2016).

other In-rich deposits with smaller metal reserves, such as the Jubankeng, Jinziwo, and Dabaoshan deposits, have also been mentioned in previous studies (Zhang et al., 2003; Tu, 2004). However, due to their small indium resources with low economic values, few studies focused on these deposits. Thus, no more detailed data about them will be presented in this paper.

2.2. *Indium deposits in the western Nanling Range and surrounding regions*

The Nanling Range, one of the most important W-Sn metallogenic province in China, hosts abundant large to superlarge Sn-W polymetallic deposits (Fig. 6) (Yuan et al., 2019; Ni et al., 2021). The indium deposits in this region are clustered in the western Nanling Range (WNR), including the Xianghualing Sn-polymetallic deposit, Yejiwei Sn-polymetallic deposit, and Qibaoshan Cu-polymetallic deposit. Early studies suggested that the indium resources hosted in the WNR are much less than those in the SYB, which results in the indium mineralization in this region to be ignored (Zhang et al., 2003). Recently, published data demonstrated that indium is significantly enriched in sphalerite from the WNR relative to the SYB (Liu et al., 2017, 2018). For example, sphalerite from the Xianghualing Sn-polymetallic deposit has the highest indium concentration (up to ~22 wt%) in China, and indium mineralization has been found in Sn-poor deposits such as the Qibaoshan Cu-polymetallic deposit (Liu, 2017; Liu et al., 2017, 2018). Thus, it is necessary to further consider In-rich deposits in the WNR, which may bring us new insights into the enrichment mechanisms of indium and provide guidance for future exploitation.

The **Xianghualing Sn-polymetallic deposit** is located in the Linwu County, Hunan Province, and the tin mineralization occurred in the northeastern part of the Tongtianmiao dome (Figs. 6 and 7a). It contains 0.13 Mt Sn, 0.17 Mt Pb + Zn, 2.8 kt WO_3, and 0.18 kt Ag; however, indium reserves have not been reported (Lai, 2014). The chemical analyses applied to different ores yield an average indium grade of 163 ppm (Liu et al., 2017). The orebodies are close to the contact zone between the Laiziling granites and Cambrian to Devonian carbonate and clastic rocks (Fig. 7b-d). Cassiterite, pyrite, galena, sphalerite, chalcopyrite, arsenopyrite, and pyrrhotite are common ore minerals in these orebodies (Fig. 7e-m). In this district, two granitic stocks (the Laiziling and Jianfengling granites) of biotite granite are intruded into the Cambrian metasandstone and Devonian carbonate, respectively (Fig. 7a). These granites are highly fractionated and peraluminous (A/CNK > 1.1), with high contents of total alkalis (6.9 wt% in average) and high 1000 Ga/Al ratios (>4), which are similar to A-type granites (Xiao et al., 2019). Zircon U–Pb dating of the Laiziling and Jianfengling granites yield ages ranging from 160.7 Ma to 150.4 Ma (Li et al., 2018; Xiao et al., 2019), indicating that they emplaced during Late Jurassic period. This result coincides with the mineralization ages obtained by cassiterite U–Pb age (156.0 Ma) and muscovite Ar-Ar age (154.4 Ma) (Yuan et al., 2007, 2008). The close spatial relationship between these granites and orebodies and the consistent ages, supports a genetic connection between Jurassic magmatism and tin mineralization. Similar to other indium deposits, sphalerite in zinc ores from the Xianghualing Sn-polymetallic deposit is the most important carrier of indium and has high average indium concentrations (1.5 wt%). Other sulfides such as chalcopyrite (0.07 wt%) and tetrahedrite (0.43 wt%; $Cu_{12}(Sb, As)_4S_{13}$) also have relatively high indium concentrations (Liu et al., 2017). Furthermore, the indium concentration of the Laiziling granite

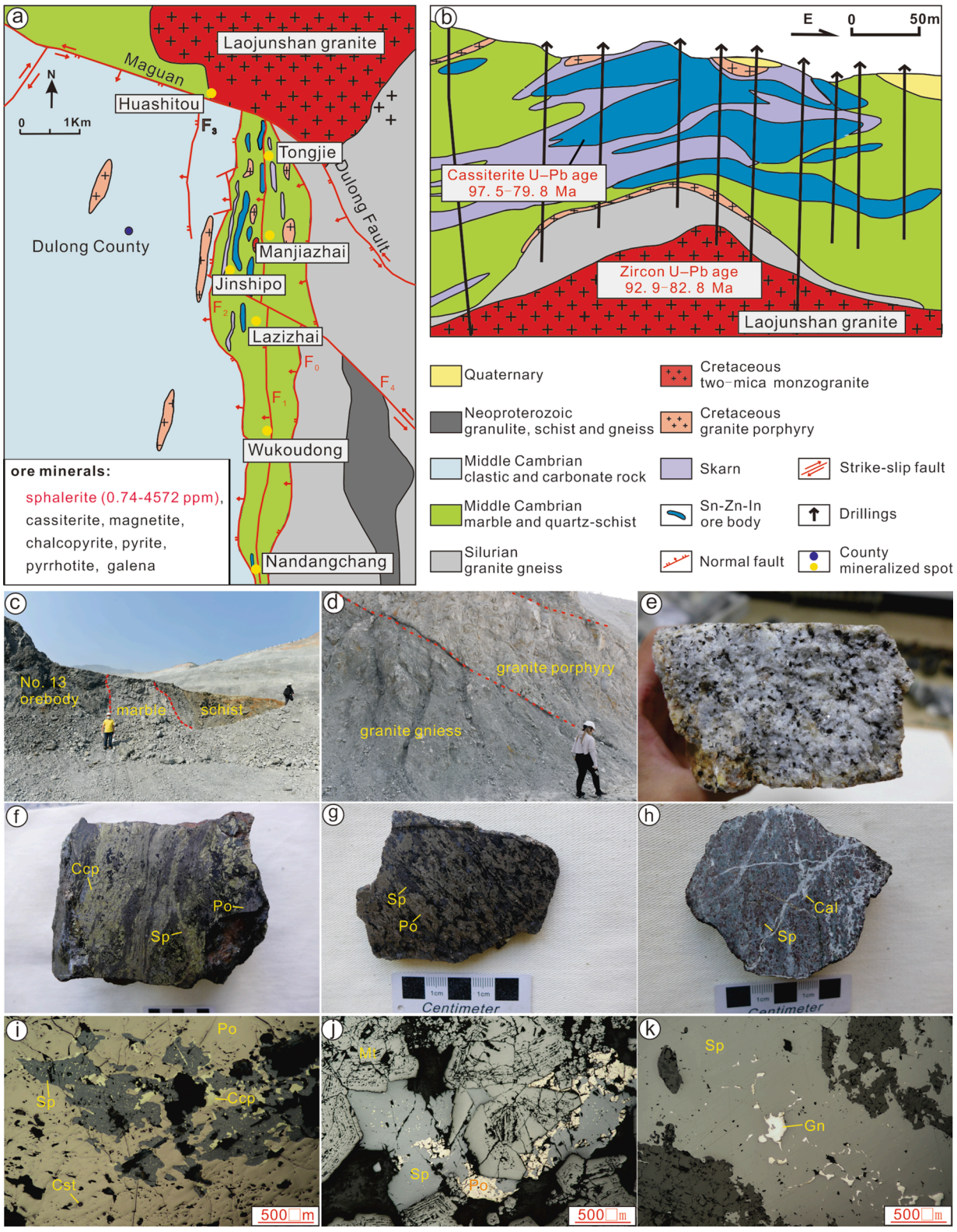

Fig. 4. (a) Geological map of the Dulong Sn-polymetallic deposit. (b) Geological cross-section along exploration line 125 (modified after Xu et al., 2015). (c-k) Photos of the outcrop, handspecimens and thin sections of the In-rich Dulong deposit: (c) No.13 orebody and its relationship with host rocks; (d) The Cretaceous granite porphyry intruding into the Silurian granite gneiss; (e) Medium- to coarse-grained two-mica monzonitic granite of the Laojunshan intrusion; (f) Sulfide ore containing sphalerite, pyrrhotite and chalcopyrite; (g) Massive sphalerite-pyrrhotite; (h) Disseminated sphalerite ore crosscut by calcite veins; (i) Sphalerite and chalcopyrite enclosed by pyrrhotite; (j) Magnetite intergrowth with sphalerite and pyrrhotite; (k) Galena randomly distributed in the sphalerite matrix. Abbreviations: Py = pyrite, Gn = galena, Sp = sphalerite, Po = pyrrhotite, Mt = magnetite, Ccp = chalcopyrite, Cal = calcite, Cst = cassiterite. Ore minerals in the Dulong deposit are listed in the insets. The In-bearing minerals and indium concentrations are highlighted by red color, and the granite associated with mineralization is labeled by "zircon U-Pb age" in red color, which is also the case in other figures.

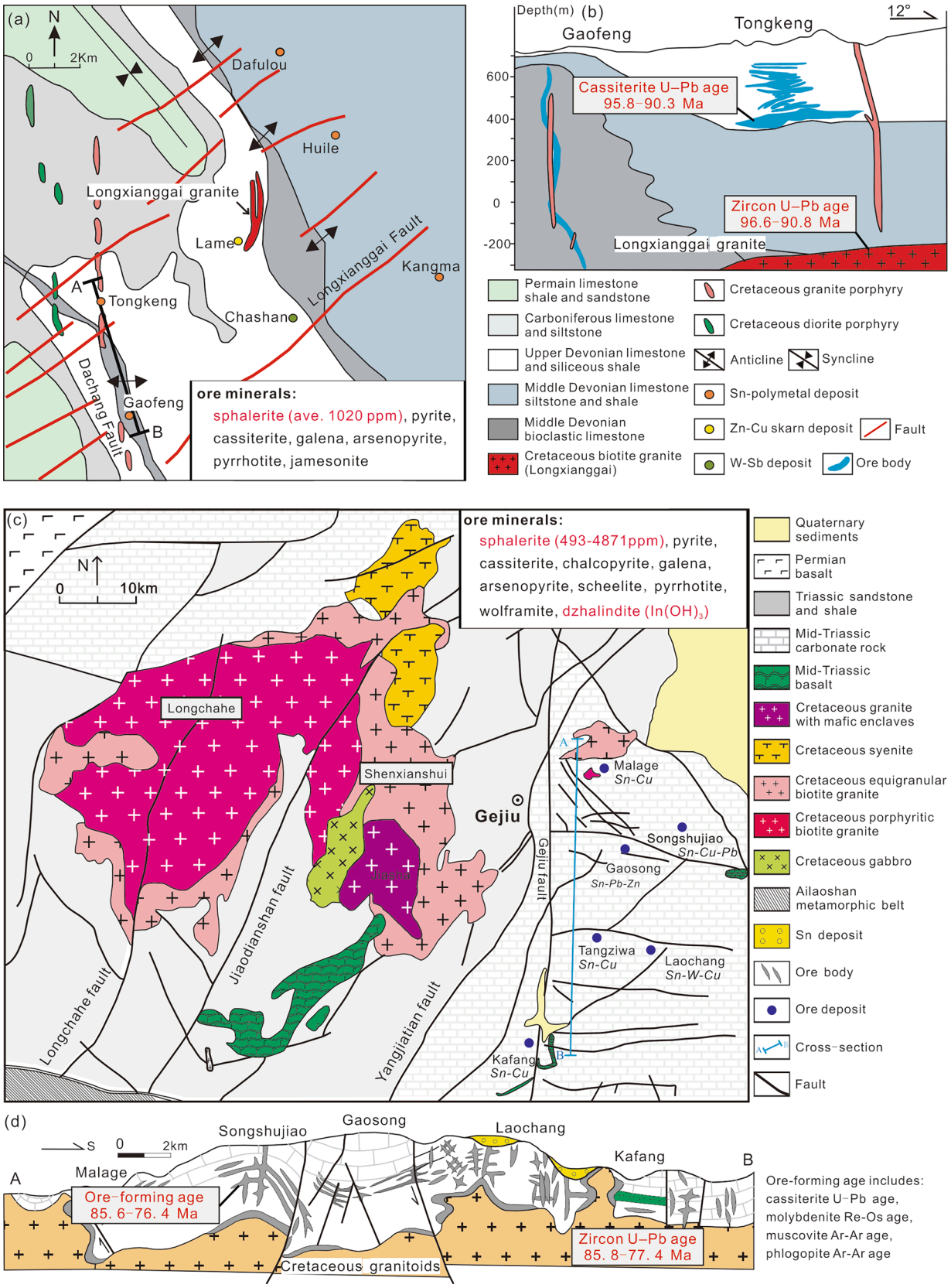

Fig. 5. (a) Geological map of the Dachang district and (b) geological cross-section along the line A-B (modified after Huang et al., 2019). (c) Geological map of the Gejiu district and (d) geological cross-section along the line A-B (modified after Li et al., 2015). The Cretaceous granitoids in (d) include all the Cretaceous ganites shown in (c).

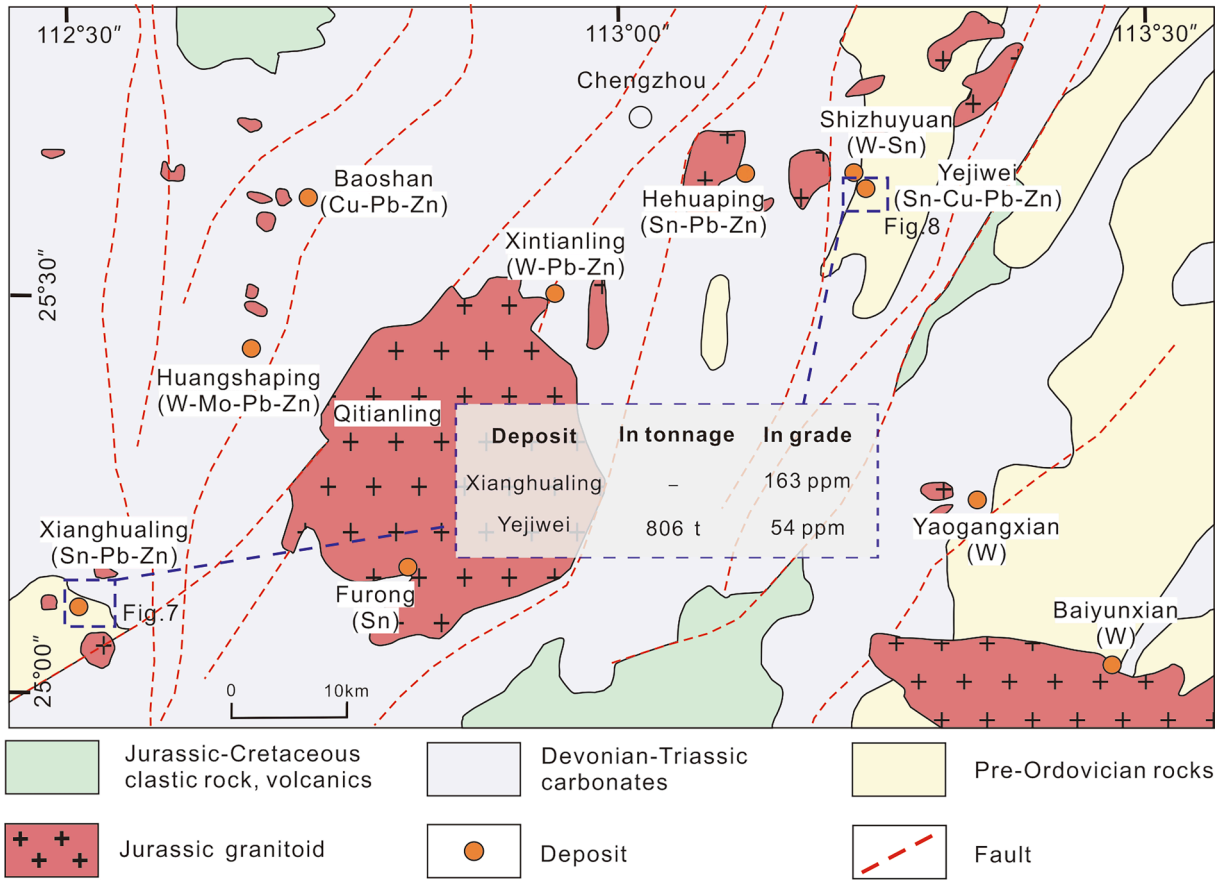

Fig. 6. Geological map showing the distribution of major deposits in the western Nanling Range (modified after Ding et al., 2018). The indium deposits in this region include the Xianghualing and Yejiwei deposit. The tonnage and grade of indium are from Liu et al. (2017) and (2018).

(0.14–0.62 ppm) is higher than that of continental crust (0.056 ppm), supporting the idea that the In-rich, A-type granite is associated with the indium mineralization in the Xianghualing Sn-polymetallic deposit (Liu et al., 2017).

The **Yejiwei Sn-polymetallic deposit,** located in the Chenzhou city, Hunan Province, is approximately 1.5 km to the southeast of the world-class Shizhuyuan Sn-polymetallic deposit (Figs. 6 and 8a). It contains 806 t In, with an average grade of 54 ppm, 0.12 Mt Sn, 66 kt Cu, 24 kt WO_3, and minor Ag, Zn, Ga, and Cd resources (Liu et al., 2018; Zhao et al., 2018a). The orebodies mainly occur around the quartz porphyry that intruded into the Devonian dolomitic limestone (Fig. 8a), where ore minerals mainly include cassiterite, pyrrhotite, arsenopyrite, chalcopyrite, pyrite, galena, and sphalerite (Fig. 8e-j). The latest muscovite Ar-Ar dating yielded a mineralization age of 154.0 Ma (Liao et al., 2021), which is consistent with the emplacement age of the quartz porphyry (152.7 Ma) (Zhao et al., 2018a). These coincident ages indicate that the polymetallic deposits in the Shizhuyuan-Yejiwei district (158.8–151.1 Ma) are genetically related to the Late Jurassic granites (160.3–148.2 Ma) (Zhao et al., 2018a). However, the enrichment of indium in this deposit is poorly documented. Available EPMA (Electron Probe Micro-analyzer) data demonstrate that sphalerite is the most important In-bearing mineral, with an average concentration of 2.6 wt% (Liu et al., 2018). The indium concentrations of the sphalerite decrease gradually from granitic intrusions outward to the contact zones, and the maximum concentration (~10 wt%) occurred in the porphyry-type ores (Liu et al., 2018). Additionally, other subordinate In-bearing minerals such as chalcopyrite (0.07 wt%) and stannite (0.15 wt%; Cu_2FeSnS_4) are also discovered in this deposit (Liu et al., 2018).

The **Qibaoshan Cu-polymetallic deposit**, located to the north of the WNR, is the largest Cu-polymetallic deposit in northeastern Hunan Province (Figs. 1 and 9) (Hu et al., 2017). It contains 659 t In, with an average grade of 57 ppm, as well as 0.28 Mt Cu, 0.57 Mt Pb + Zn, 0.47 Mt Mn, 31 t Au, >2.0 kt Ag, 2.8 kt Cd, 0.71 kt Ge, 1.1 kt Te, and 1.2 kt Ga (Liu, 2017; Yuan et al., 2018). Field investigations suggest that the orebodies are dominantly hosted in the altered quartz porphyry and Carboniferous dolomitic limestone (Fig. 9 a-c). These orebodies are mainly composed of ore minerals, such as pyrite, chalcopyrite, sphalerite, marcasite (FeS_2), and lillianite ($Pb_3Bi_2S_6$) (Fig. 9 d-i). In the ore field, well-developed EW-trending faults control the emplacement of magma (Hu et al., 2017). The Qibaoshan quartz porphyry was characterized by high content of Al_2O_3, high K_2O/Na_2O ratios, and high zircon $\delta^{18}O$ values (8.4 to 10.8‰), indicating that it was generated by the partial melting of ancient crust and is similar to S-type granite (Yuan et al., 2018). Zircon U–Pb dating indicates that the Qibaoshan quartz porphyry was emplaced between 154.8 and 148.3 Ma (Hu et al., 2016; Yuan et al., 2018), which is consistent with the mineralization age constrained from Rb-Sr dating of ore-bearing quartz veins (153.4 Ma, Hu et al., 2017) and molybdenite Re-Os dating (153.2 Ma, Yuan et al., 2018). Different from other Sn-polymetallic deposits with indium enrichment, ores from the Qibaoshan Cu-polymetallic deposit are Sn-poor (the Sn concentrations are lower than 70 ppm), and no tin minerals have been found in this deposit. However, the average indium concentration can be as high as 123 ppm in the sphalerite-pyrite ores, where sphalerite with indium concentrations up to 0.10 wt% is the main carrier of indium (Liu, 2017). This is the first report that indium mineralization has been found in Sn-poor deposit.

Recently, In-bearing deposits were also reported in the Xiangxi-Qiandong Pb-Zn metallogenic belt (Fig. 1), where the indium grades of the polymetallic vein-type ores range from 4.8 to 189 ppm (Zhou et al., 2017). Although no mineralization-related intrusions were

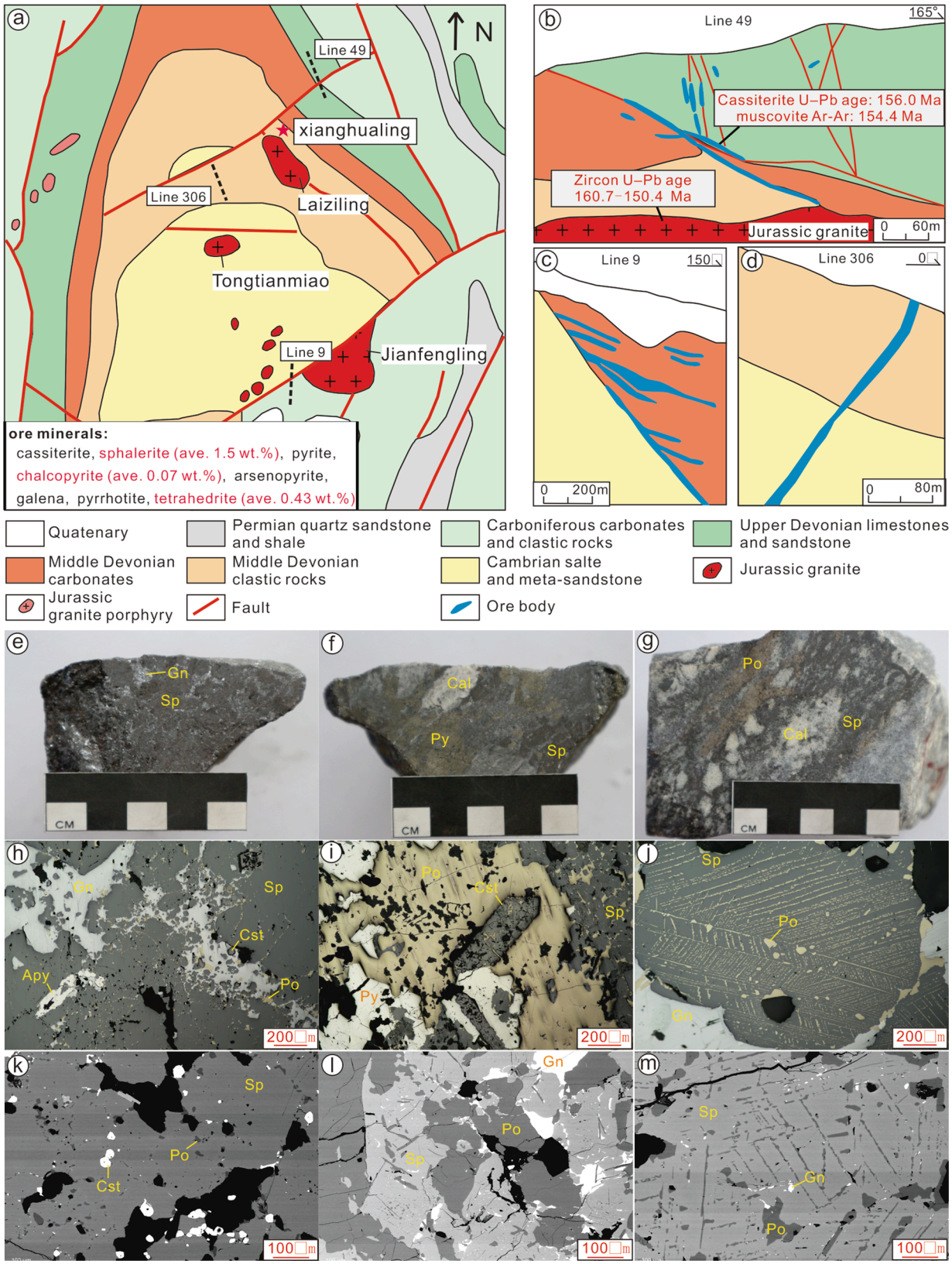

Fig. 7. (a) Geological map of the Xianghualing district. (b-d) Geological cross-sections along exploration lines 49, 9, and 306, respectively (modified after Liu et al., 2017). (e-m) Photographs of hand specimens and thin sections from the Xianghualing deposit: (e) Massive sulfide ore containing sphalerite and galena. (f) Massive sphalerite- pyrite ore. (g) Dense disseminated sulfide ore with sphalerite replacing the calcite of the host rock. (h) Galena replaces the early sphalerite that contains inclusions of pyrrhotite, arsenopyrite, and cassiterite. (i) Euhedral cassiterite and sphalerite were replaced by pyrrhotite and pyrite. (j) Sphalerite coexisting with galena contains pyrrhotite showing exsolution texture. (k) Abundant pyrrhotite and cassiterite inclusions in sphalerite (backscattered electron image). (l) Sphalerite and galena are co-crystalized with pyrrhotite. (m) Sphalerite contains the exsolutions of pyrrhotite and galena inclusions. Abbreviation: Py = pyrite, Apy = arsenopyrite, Gn = galena, Sp = sphalerite, Po = pyrrhotite, Cal = calcite, Cst = cassiterite.

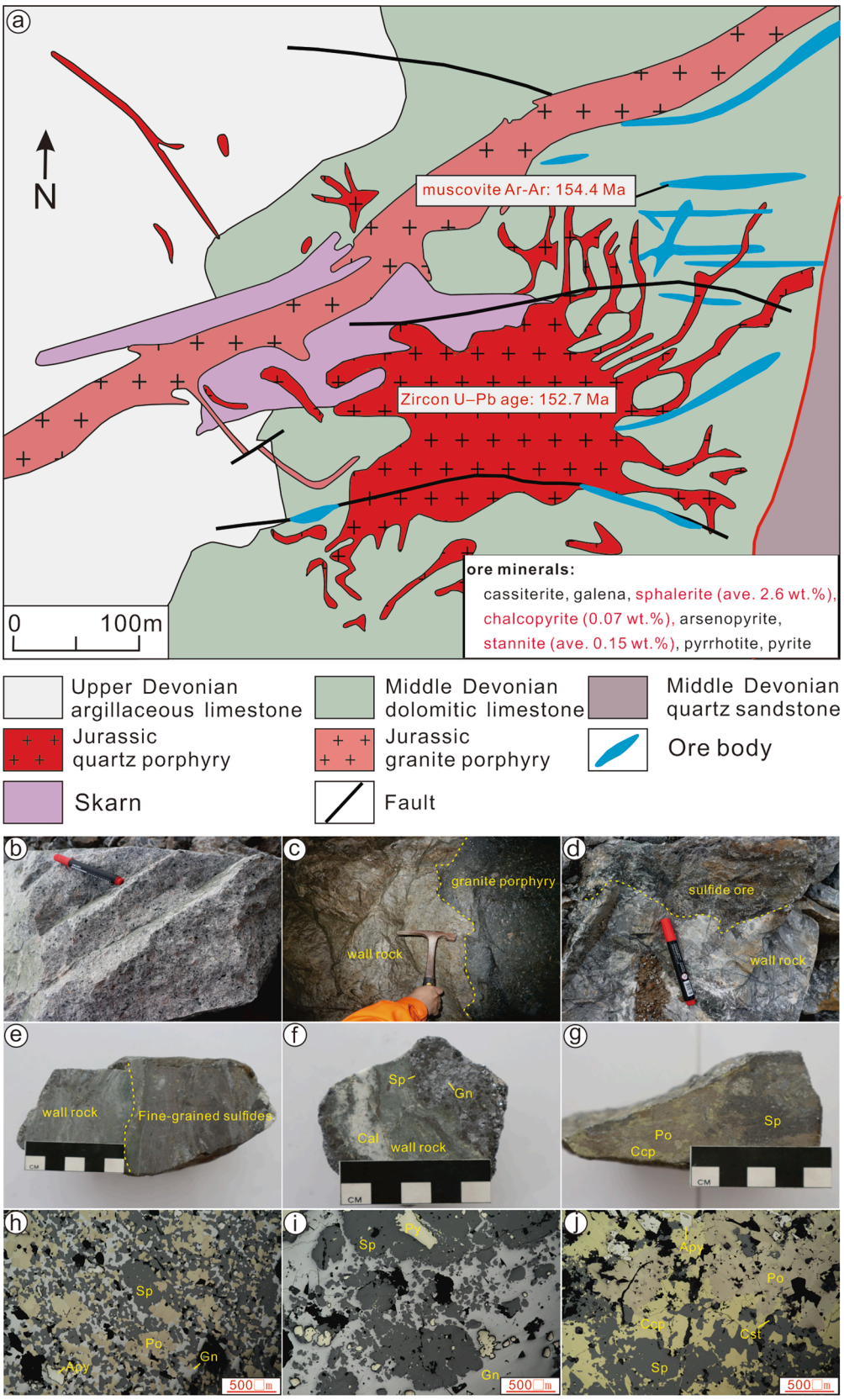

Fig. 8. (a) Geological map of the Yejiwei Sn-polymetallic deposit in the western Nanling Range (modified after Zhao et al., 2018a). (b-j) Photographs of outcrops, hand specimens, and thin sections of ores from the Yejiwei deposit. (b) Granite porphyry; (c) The boundary between the wall rock and granite porphyry. (d-e) The boundary between the wall rock and sulfide ore. (f-g) The mineralized wall rock is crosscut by a calcite vein and the sulfides include galena and sphalerite. (h) Photomicrographs of the fine-grained sulfides in (e), showing that the sulfides are composed of galena, pyrite, sphalerite, and pyrrhotite. (j) Sphalerite and pyrite are replaced and cemented by galena. (k) Chalcopyrite replaces sphalerite, arsenopyrite, and pyrrhotite. Abbreviations: Py = pyrite, Apy = arsenopyrite, Gn = galena, Sp = sphalerite, Po = pyrrhotite, Ccp = chalcopyrite, Cal = calcite, Cst = cassiterite.

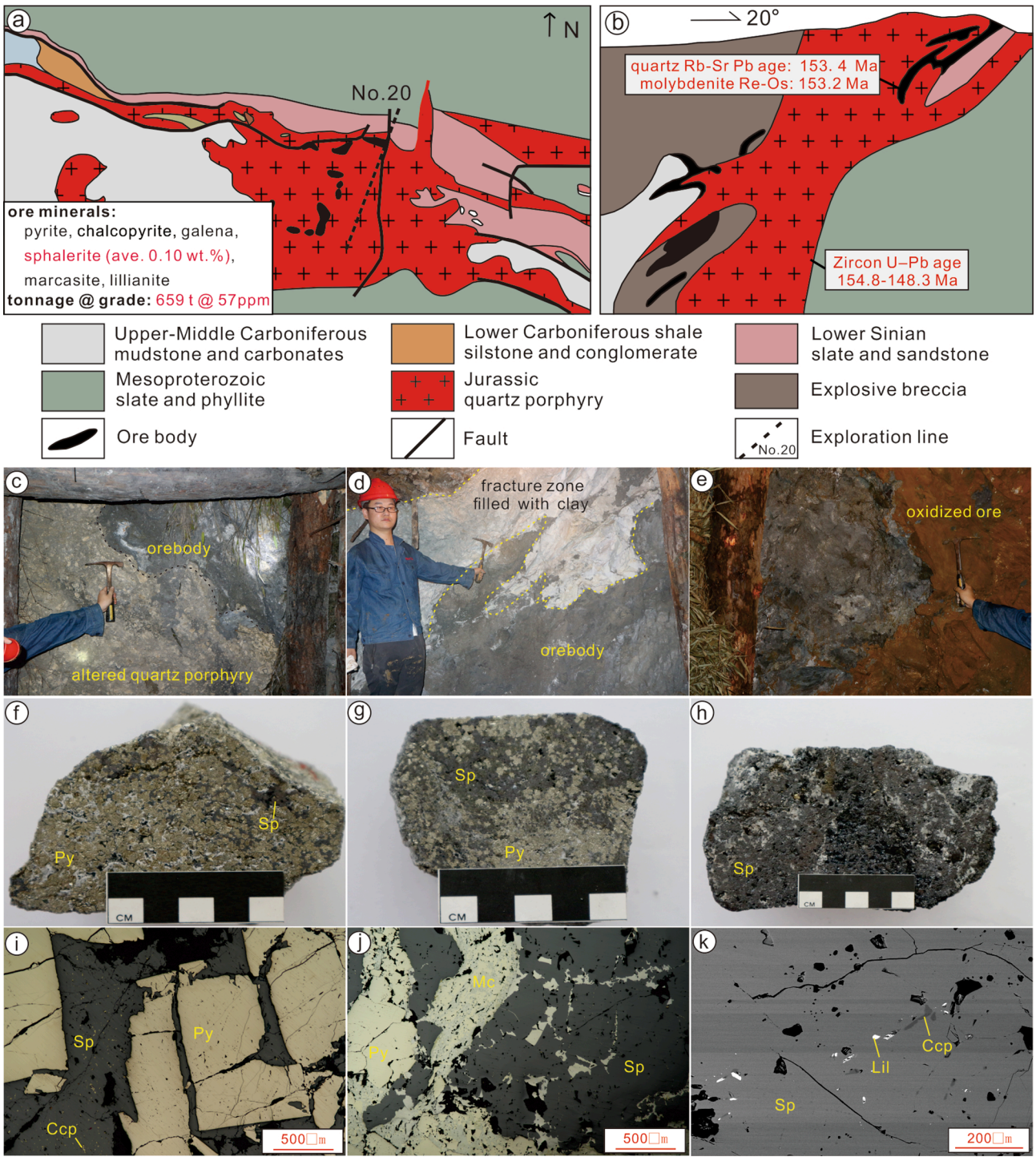

Fig. 9. (a) Geological map of the Qibaoshan Cu-polymetallic deposit. The tonnage and grade of indium are from Liu (2017) and Yuan et al. (2018). (b) Geological cross-section along exploration line 20 (modified after Yuan et al., 2018). (c-k) Photographs of outcrops, hand specimens, and thin sections from the Qibaoshan deposit. (c) Sulfide orebody and its relationship with altered quartz porphyry. (d) Sulfide orebody is crosscut by the fracture zone filled with clay. (e) Oxidized orebody. (f-g) Dense disseminated sulfide ore containing sphalerite and pyrite. (h) Porous sphalerite dominated ore. (i) Granular pyrites are cemented by sphalerite containing chalcopyrite inclusions. (j) Marcasite replaces pyrite and sphalerite. (k) Sphalerite contains lillianite and chalcopyrite inclusions. Abbreviations: Py = pyrite, Apy = arsenopyrite, Sp = sphalerite, Ccp = chalcopyrite, Mc = marcasite, Lil = lillianite.

discovered in Pb-Zn ore field, geophysical data suggest that there are hidden intrusions at depth (Zhou and Wen, 2021). Thus, Zhou et al. (2017) suggests that the metallogenic belt potentially contains unexplored granite-related high-temperature Sn-Cu-In sulfide deposits. However, the genesis of these deposits remains unclear due to a lack of precise geochronological constraints. Previous work on Au deposits (eg. the Pinqiu and jinjing Au deposits) and MVT (Mississippi Valley-Type) Zn-Pb deposits (eg. the Shizishan Pb-Zn deposit) showed that there are multiple mineralization events in this region during Paleo-Caledonian (Wang et al., 2011; Duan et al., 2014). This result indicated that these deposits, including In-bearing Pb-Zn deposits, may be related to the Guangxi Orogeny (a significant tectonic-thermal event during 460–405

Ma in the SYB) (Zhou and Wen, 2021). Therefore, the Paleo-Caledonian may be another important period for indium mineralization in China, and vein-type Pb-Zn deposits in the Xiangxi-Qiandong metallogenic belt may be a potential source of indium.

2.3. Indium deposits in the southern Great Xing'an Range

The southern Great Xing'an Range (SGXR) is located in the northeastern part of the mainland China, where multistage tectonic-magmatic activities and mineralization events have been recognized (Zeng et al., 2016). Recently, a series of Late Jurassic-Early Cretaceous Sn-polymetallic deposits have been discovered in the SGXR (Fig. 10) (Mao et al., 2019b). Mao et al. (2018, 2019a, 2021) suggested that the Sn-polymetallic deposits in the SGXR are similar to those in the Bolivian tin metallogenic belt, in terms of geology, alteration and mineralization style, and tectonic environment. Considering the latter is the most important In-rich ore belt in the world (Xu and Li, 2018; Torró et al., 2019), the SGXR may has great resource potential for indium like the Bolivian tin metallogenic belt. Several In-rich deposits, including the Meng'entaolegai, Dajing, Budunhua, Baiyinuo'er, Naoniushan, and Aonaodaba Sn-Pn-Zn-Ag polymetallic deposits have been reported in the literature (Tu, 2004); however, most of these deposits are poorly studied and only the Meng'entaolegai and Dajing deposits are well documented (Zhang et al., 2004, 2006; Ishihara et al., 2008).

The **Meng'entaolegai Ag-polymetallic deposit**, located in the eastern Inner Mongolia, has a mining history beginning in the 1950s (Fig. 10b-d). It contains >500 t In, with an average grade of 118 ppm, as well as 0.16 Mt Pb, 0.3 Mt Zn, 3.0 kt Sn, 2.0 kt Ag, and 1.8 kt Cd (Zhang et al., 2006). In the ore field, orebodies mainly occur as polymetallic sulfide veins controlled by E-W-trending faults (Fig. 10d), and ore minerals mainly include galena, sphalerite, pyrite, chalcopyrite, arsenopyrite, cassiterite, stannite, and Ag minerals (Zhang et al., 2004, 2006). The magmatic intrusions in this district include the Duerji granite and Meng'entaolegai granite, of which the former is mainly composed of biotite granite and the latter comprise biotite granite and muscovite granite (Song et al., 2014). Although orebodies are mainly hosted in the Meng'entaolegai granite batholith, the mineralization age constrained from muscovite Ar-Ar dating (179.0 Ma, Zhang et al., 2003) is inconsistent with the emplacement age of Meng'entaolegai (240.5–234.3 Ma) and Duerji granites (154.5 Ma) (Song et al., 2014). The $\delta^{34}S$ and $\delta^{18}O$ values of sulfides and fluid inclusions from this deposit range from −1.7‰ to 4.6‰ and 4.8‰ to 7.9‰, respectively, suggesting that the ore-forming fluids may originate directly from a magmatic system (Zhu et al., 2004). However, because the Pb isotopic composition of the ores ($^{206}Pb/^{204}Pb$ 18.131–18.308, $^{207}Pb/^{204}Pb$ 15.421–15.564, $^{208}Pb/^{204}Pb$ 37.690–38.116) is quite different from those of the granites ($^{206}Pb/^{204}Pb$ 18.460–19.445, $^{207}Pb/^{204}Pb$ 15.514–15.607, $^{208}Pb/^{204}Pb$ 38.003–38.932) in this region, Zhang et al. (2002) suggested that the mineralization is likely related to a concealed intrusion emplaced during the Jurassic periods. Because metal resources have been exhausted, research on the Meng'entaolegai deposit is hampered. Available data show that the indium concentrations of sphalerite from this deposit range from 85 to 2660 ppm and increase with the mineralization temperature (Zhang et al., 2004, 2006).

The **Dajing Sn-Cu polymetallic deposit**, located in the Linxi County, Inner Mongolia, is a large polymetallic deposit containing 1.5 Mt Zn, 0.30 Mt Pb, 0.30 Mt Cu, 75 kt Sn, and 3.3 kt Ag, as well 768 t In in an average grade of 112 ppm (Fig. 10f-h) (Ishihara et al., 2008; Wang et al., 2015). Ore veins in this deposit are mainly hosted by Permian sandstone, and comprise ore minerals such as pyrite, pyrrhotite, arsenopyrite, cassiterite, chalcopyrite, sphalerite, and galena (Liu et al., 2019). In the Dajing district, zircon U–Pb dating is consistent with magmatic activity at 253.8–239.0 Ma and 170.7–162.0 Ma and represented by E-W-striking dikes (Jiang et al., 2012). These results are inconsistent with the mineralization ages constrained from sericite Ar-Ar dating (138.0 Ma) and cassiterite U–Pb dating (144.0 Ma) (Liao et al., 2014). However, some igneous rocks with eruption/emplacement ages of 144.0–146.0 Ma were discovered in the peripheral district, suggesting that the Dajing deposit could be genetically related to a concealed granite emplaced at ~140.0 Ma (Jiang et al., 2012; Liao et al., 2014). Due to the absence of geochemical data on ore minerals, the occurrence of indium is still unclear. However, the chemical compositions of ores show that indium is poorly correlated with zinc ($R = 0.05$) but better correlated with copper ($R = 0.65$) (Ishihara et al., 2008). Moreover, the indium contents of copper concentrates are higher than that of zinc concentrates, suggesting that indium may be incorporated into copper sulfide (and/or sulfosalt) rather than sphalerite (Ishihara et al., 2008). Fluid inclusion studies suggested that the composition of ore-forming fluids are extremely complex and sourced from three fluid systems: a mantle-derived, Cu-rich fluid; a crust-derived, Sn-rich fluid; and low-temperature Pb-Zn-Ag-rich fluid (Wang et al., 2015; Liu et al., 2019). So far, it remains unclear which fluid is responsible for indium mineralization in this deposit.

2.4. Indium mineralization in other regions

In addition to the indium deposits described above, there are some In-bearing deposits reported in other regions. For example, Liu et al. (1998) reported some In-bearing gold ores (5.0–17 ppm) in western Qinling. Guo et al. (2006) noted that the Chahe Sn-polymetallic in Sichuan Province contains considerable indium resources, with the highest grade reaching up to 187 ppm indium. In Tibet, two indium minerals, native indium (In) and dzhalindite, were reported by Zhao et al. (2010) in the Bangong-Nujiang copper polymetallic metallogenic belt. The Lawu Cu-Pb-Zn polymetallic deposit located in this belt has an average indium grade of 45 ppm. In Fujian Province, the Zhongjia Sn-polymetallic deposit has an estimated 569 t indium with an average grade of 76 ppm (Mao et al., 2013) and in the Zijinshan Cu-Au deposit, roquesite ($CuInS_2$) has been reported (Wang et al., 2014). In Qinghai Province, roquesite was reported in the Saishitang-Rilonggou Cu-Sn ore field, and 136 t indium was estimated there (Liu et al., 2016; Wang et al., 2016). All these findings suggest that China may have great resource potential for indium, and more efforts should be put into these newly discovered In-bearing deposits.

3. Indium occurrence in minerals

Identifying the indium occurrence in minerals is crucial for understanding the incorporation and enrichment mechanism of indium. In most indium deposits in China, sphalerite is the most important carrier of indium. To date, indium minerals have only been reported in a few deposits: (1) Roquesite occurs in the Zijinshan Cu-Au deposit and Cu-Sn skarn ores in the Saishitang-Rilonggou ore field, which is consistent with a relatively high-temperature and Cu-rich environment (Wang et al., 2014; Liu et al., 2016). (2) Native indium and dzhalindite were reported in skarn Cu-Fe deposits in Tibet, where native indium is hosted in calcite and sphalerite, while dzhalindite is mainly hosted in quartz. Dzhalindite, as a common indium mineral in supergene environments, has also been found in the oxidized ores of the Gejiu deposit (Zhao et al. 2010; Li et al., 2015). (3) Damiaoite ($PtIn_2$) and yixumite (Pt_3In) were first discovered by Yu (1997a, 1997b) in the Damiao Fe deposit, Hebei Province. Generally, vermicular damiaoites are exsolved from spherical yixumite, or yixumite is enclosed by damiaoite (Yu, 1997a, 1997b). Although the SYB hosts abundant indium resources, no indium minerals are found in primary ores. This may be attributed to the presence of abundant sphalerites that sequester indium in its structure and inhibit the formation of indium minerals.

In the past two decades, *in-situ* analysis techniques, such as LA-ICP-MS and EPMA, have been widely applied to investigate the occurrence of indium in sphalerite. It has been revealed that indium is homogeneously distributed in sphalerite from the SYB and shows a positive correlation with copper, corroborating the coupled substitution of In^{3+}

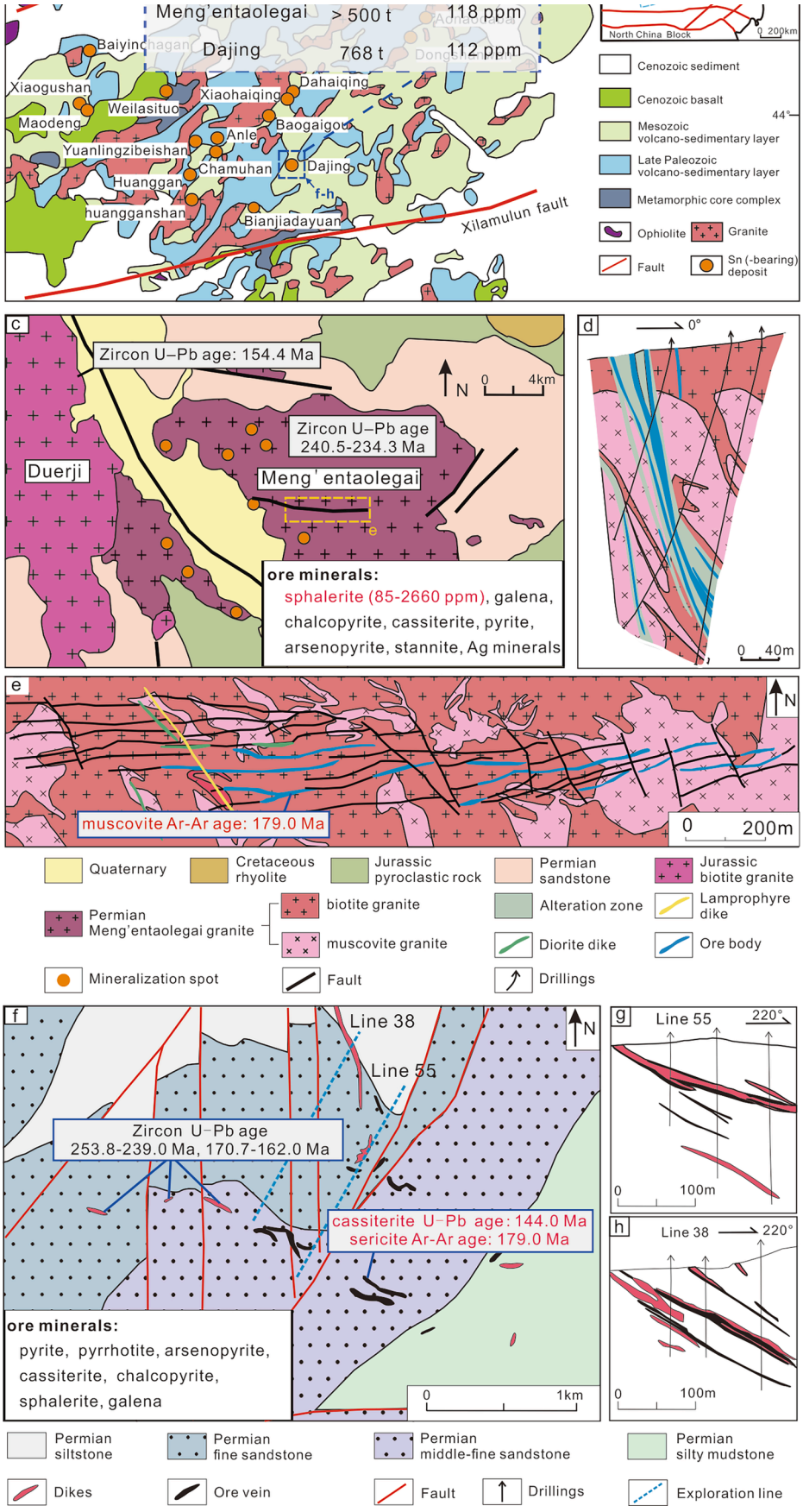

Fig. 10. (a) Simple tectonic map and (b) the distribution of major deposits in the southern Great Xing'an Range (modified after Mao et al., 2019). The Meng'entaolegai and Dajing deposits are the primary indium deposits in this region. The tonnage and grade of indium are from Zhang et al. (2006) and Ishihara et al. (2008). (c) Geological map of granites in the Meng'entaolegai district, and (d) the Meng'entaolegai Ag-polymetallic deposit. (e) The geological cross-section of representative orebodies (modified after Zhang et al., 2006). (f) Geological map of the Dajing Sn-polymetallic deposit and (g-h) geological cross-section along exploration lines 55 and 38 (modified after Yuan et al., 2018). The tonnage and grade of indium are from Zhang et al. (2006) and Ishihara et al. (2008). Note no granites are labeled by "zircon U-Pb age" in red color due to the ore-related intrusions being ambiguous in this region. Similarly, no mineral is marked in red in (f) due to a lack of geochemical data on ore minerals.

$+ Cu^{+} \leftrightarrow 2Zn^{2+}$ (Murakami and Ishihara, 2013; Li et al., 2015; Xu et al., 2021b). This substitution mechanism was directly observed in In-rich sphalerite blebs from the Dulong deposit using high-angle annular dark field scanning transmission electron microscopy (HAADF STEM) (Xu et al., 2021a). In addition to copper, charge balance can also be achieved by involving minor silver (with an oxidation of +1) in sphalerite structure (Trofimov et al., 2020). Based on the results of the atom probe and Kuchi diffraction analyses, Krause et al. (2020) further proposed that indium and copper could exist as discrete exsolved nanophases in sphalerite. Recently, some sphalerites with an atomic In/Cu ratio greater than 1 were discovered in the Dachang deposit, suggesting the existence of In-rich nanoparticles in these sphalerites (Pi et al., 2019), but more research is needed to support this hypothesis.

Compared with sphalerite from the SYB, sphalerite from the WNR has higher indium concentrations, and indium is heterogeneously distributed in sphalerite grains. In the Xianghualing deposit, indium concentrations can reach 7.0–8.0 wt% in the core of sphalerite and ~22 wt% in the rim (Liu et al., 2017). The extremely high indium concentrations in sphalerite from this region likely resulted from the In-rich ore-forming fluid (Valkama et al., 2016b; Liu et al., 2017). However, because of a shortage of Zn in the WNR, a large amount of indium was sequestered by limited sphalerite, resulting in an exceptional enrichment of indium in its structure. Consequently, it can be deduced that indium minerals are more likely to be found in the WNR relative to the SYB.

4. The characteristics of In-bearing magmatic-hydrothermal systems

4.1. Characteristics and genesis of granitic intrusions

Indium is moderately to highly incompatible during partial melting, and tends to concentrate in highly fractionated magma (Sun, 1982; Liu et al., 1984). Almost all the indium deposits in China are related to A/S-type granites, suggesting that these granites may play an important role in indium enrichment.

Currently, the indium resources in China are primarily sourced from Sn-polymetallic deposits, which is consistent with strong correlation between indium and tin. According to previous studies, the granites associated with tin mineralization in South China are generated by partial melting of argillaceous sedimentary rocks (Fig. 11a) and are peraluminous, highly fractionated, and volatile-rich (Yuan et al., 2019; Mao et al., 2019b). Because of the low mobility of indium during chemical weathering, it tends to remain in weathered rocks (Liu et al., 1984; Lopez et al., 2015). Similarly, tin is also immobile in surficial environments and easily adsorbed by clay minerals in sediments (Romer and Kroner, 2014, 2016), which can form biotite- and muscovite-rich metamorphic mineral assemblages via prograde metamorphism (Wolf et al., 2018).

Previous studies (Liu et al., 1984; Gion et al., 2018; Wang et al. 2019) suggest that biotite is an important carrier of indium and tin. If melt generation is controlled by biotite-dehydration melting, indium and tin could be synchronously released into the melt. However, the breakdown of biotite would need to occur at temperatures > 800 °C (Wolf et al., 2018). Mao et al. (2019b) and Yuan et al. (2019) systematically summarized the geochemical characteristics of granites in South China, and found that the formation Sn-mineralized granite is controlled by biotite-dehydration melting under high temperature (800 ± 20 °C). However, the heat generated by the thickening of the crust is not enough to support the biotite-dehydration melting (Clark et al., 2011; Zhao et al., 2022a). Such high temperature requires the input of additional heat from the mantle. This extensive existence of mantle-derived mafic microgranular enclaves and mafic/ultramafic dikes in many Sn-polymetallic deposits in South China supports external heating by interaction with mantle material (Zhao et al., 2022b). Therefore, biotite-dehydration melting triggered by mantle-derived heat could be a crucial process for Sn-In mineralization (Yuan et al., 2019; Jiang et al., 2020; Sui et al., 2020).

Based on the study of the Mesozoic deposits and granites in South China, previous studies proposed that the magmatic and metallogenic belts in the SYB and WNR were controlled by the subduction of the Neo-Tethys Plate and Paleo-Pacific plate, respectively (Zhang et al., 2017, 2018; Xu et al., 2018; Huang et al., 2019). Because of roll-back of the oceanic slab during subduction, additional heat could be brought from the mantle into the crust during asthenosphere upwelling, resulting in the breakdown of biotite in the metasedimentary crust and release of indium and tin. Indeed, besides indium and tin, biotite is also a main carrier of barium, while muscovite is a main carrier of lead in metasedimentary rock. If melt is generated by biotite-dehydration melting, the melt will display a lower Pb/Ba ratio; otherwise, the Pb/Ba ratio of melt will be elevated once the partial melting is controlled by muscovite-dehydration melting (Finger and Schiller, 2012). In the Pb-Ba diagram (Fig. 11b), the ore-related granites from the SYB mainly plot in the field of biotite-dehydration melting, whereas ore-related granites in the WNR mainly plot in the field of muscovite-dehydration melting. Considering biotite-controlled melting are responsible for the Sn-In mineralizations (Yuan et al.,2019; Zhao et al., 2022a), the indium resource hosted in the SYB is more abundant than that in the WNR. Thus, the origin of the source magma has a great influence on the indium enrichment.

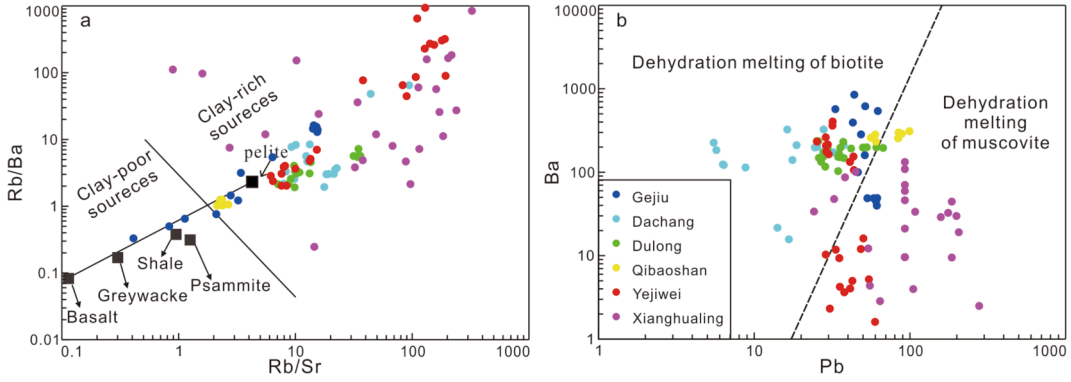

Fig. 11. Plots of (a) Rb/Ba versus Rb/Sr (after Sylvester, 1998) and (b) Pb versus Ba for granites from the major In-rich deposits in China. Line in 11b is after Finger and Schiller (2012), which delineates the fileds of the granites with low Pb/Ba ratio (labeled as biotite-dehydration melting in this study) and high Pb/Ba ratio (labeled as muscovite-dehydration melting in this study). More explanations are included in main text. (Data are sourced from Guo et al., 2015; Li et al., 2018; Guo et al., 2018a, 2018b; Zhao et al., 2018b; Yuan et al., 2018).

4.2. Characteristics of ore-forming fluid

The characteristics of ore-forming fluids, such as temperature and compositions, are crucial to understand the ore-forming processes. Because indium generally occurs as a trace element in sulfide ores, previous studies on fluid inclusions have paid little attention to indium mineralization.

Combined with the field observations, the temperature of ore-forming fluid is considered as a key factor controlling the enrichment of indium (Zhang et al., 2006). Indium is significantly concentrated in the granite-proximal locations (Wu, 2009; Guo et al., 2020). Based on the published fluid inclusion data of In-rich deposits, Zhang et al. (2003) proposed that the indium grades of ores increase with mineralization temperatures from 190 °C to 350 °C, and 250–320 °C is the most favorable temperature range, which is similar to the mineralization temperature obtained from other In-rich deposits worldwide (Shimizu and Kato, 1991; Schwarz-Schampera and Herzig, 2002; Jovic et al., 2011; Shimizu and Morishita, 2012; Torró et al., 2019).

In addition, the composition of ore-forming fluids seems to be another important control on the enrichment of indium. Previous studies have suggested that indium is preferentially concentrated in Sn-rich deposits, while Sn-poor deposits generally have much lower indium concentrations (<10 ppm) in their ore-forming fluids (Zhang, 1987, 1998; Zhu et al., 2006; Yuan et al., 2020). Therefore, Zhang et al. (2007) suggested that the presence of tin is vital for indium enrichment. Recently, a positive correlation between indium and tin was also observed in fresh granites, altered rocks, and skarn minerals from several indium deposits in China (Wang et al., 2019). LA-ICP-MS analysis of fluid inclusions also revealed various indium concentrations from 0.2 ppm to 20 ppm in high-temperature magmatic-hydrothermal fluids (350–700 °C), and the highest indium concentration (up to 34 ppm) of fluid inclusions was observed in Sn-W-mineralized granites (Audetat and Zhang, 2019). Overall, one striking feature is that the indium deposits are characterized by high tin concentrations in their ore-forming fluid system.

In addition to tin, other metal elements, such as Cu, Zn, Fe, and Cd, also have a great influence on the enrichment of indium. Indium is generally substituted into sphalerite via a coupled substitution with copper ($Cu^{+} + In^{3+} \leftrightarrow 2Zn^{2+}$), thus availability of copper in the mineralizing fluids is important to indium enrichment in sphalerite (Cook et al., 2012; Shimizu and Morishita, 2012; Andersen et al., 2016; Frenzel et al., 2016; Torró et al., 2019). In indium-rich deposits, precipitation of indium minerals occurs when the indium concentration is high enough to exceed the substitution capacity of sphalerite (Cook et al., 2011). An In (ppm)/Zn (%) ratio > 50 and indium grade > 40 ppm were proposed as limiting conditions for the formation of indium minerals (Valkama et al., 2016a, 2016b). The effect of iron on the indium enrichment is highlighted by the high indium content of Fe-rich sphalerite (Seifert and Sandmann, 2006; Pavlova et al., 2015; Li et al., 2015). The relationship between indium and cadmium is clearly shown by the "indium window", in which indium is highly concentrated in sphalerites with 0.2–0.6 wt% cadmium (Dill et al., 2013). Therefore, the ore-forming fluid of In-rich deposits is very complex, which is consistent with the fact that indium is always associated with polymetallic deposits rather than deposits dominated by single metal resources. Further studies on ore-forming processes, including fluid- and melt-inclusions from causative intrusions and ore mineral assemblages, need to be further considered to reveal the transport and participation mechanism of indium in metal-rich fluid systems.

5. Behaviors of indium in magmatic-hydrothermal system

5.1. The behavior of indium during magma evolution

The behavior of indium in magmatic-hydrothermal systems remains poorly understood. Because In^{3+} can substitute for Fe^{2+} in ferromagnesian phases (Liu et al., 1984), the probability of indium mineralization decreases as the proportion of ferromagnesian minerals increases in associated granites. In granitic melt, biotite and amphibole are the common ferromagnesian phases, thus it is important to assess the partitioning behavior of indium between them and granitic melt. Experiments conducted by Gion et al. (2018) determined the partition coefficients for indium between biotite ($D_{In}^{Bt/Melt}$), amphibole ($D_{In}^{Amp/Melt}$) and melt. They found that $D_{In}^{Bt/Melt}$ is a function of biotite compositions and ranges from 0.6 ± 0.1 to 16 ± 3. As the proportion of Fe^{2+} in the octahedral site and tetrahedral aluminum increases, the $D_{In}^{Bt/Melt}$ decreases. However, the compositions of amphibole have a minor influence on $D_{In}^{Amp/Melt}$ (36 ± 4). Because I-type granites commonly contain amphibole which can sequester a large amount of indium and prevent it from significantly concentrating in ore-forming fluid, the possibility of indium mineralization of I-type granite is lower than that of S- and A-type granites (Gion et al., 2019). Wang et al. (2019) examined the behavior of indium in granites from the SYB and WNR, and found that the $D_{In}^{Bt/Melt}$ shows a decreasing trend with granitic magma evolution, which is consistent with the observations that indium mineralization is always associated with highly fractionated granites.

In addition, volatiles (F, Cl, B, P, etc.) in the melt play an important role in both magma genesis and indium mineralization (Moura et al., 2014; Simons et al., 2017). Volatiles can effectively reduce the viscosity of the magma while increasing ion diffusivity and they can decrease the solidus temperatures and change the eutectic compositions (Keppler and Wyllie, 1991; London, 1997). Research by Simons et al. (2017) revealed elevated contents of indium in the peraluminous granites of the Cornubian batholith with increasing contents of F, Li, and P. Moreover, the existence of volatiles can reduce the proportion of bridging oxygen and increase the solubility of water in the melt, which is favorable for elements to enter the melt with high activity coefficients during partial melting (Hu et al., 2009; Sui et al., 2020; Gion et al., 2019). When the magmatic-hydrothermal fluids exsolve from the metal-rich magma, volatiles such as F^{-} and Cl^{-} can combine with metal elements to form stable complexes and then migrate together (see below).

5.2. Behaviors of indium in hydrothermal fluid

According to the classification of soft-hard acids and bases (Pearson, 1963), In^{3+} is relatively hard and can complex with hard ligands such as F^{-}, OH^{-}, Cl^{-} and SO_4^{2-} (Wood and Samson, 2006). The experiment conducted by Seward et al. (2000) showed that In^{3+} mainly existed as stable chloride ($InCl_4^{-}$) and hydroxide ($InClOH^{-}$) complexes in hydrothermal fluids, and $InCl_4^{-}$ was the dominant species at 300 °C to 350 °C (Seward et al., 2000). Similar to indium, tin also tends to complex with chlorine in aqueous fluids (Hu et al., 2009; Zhao et al., 2022c). It is widely accepted that these two elements can migrate efficiently in chlorine-rich ore-forming fluids. However, it is noteworthy that most Sn-In-related granites are highly fractioned and F-rich (Moura et al., 2014; Valkama et al., 2016a, 2016b; Simons et al., 2017; Ivashchenko, 2021). As proposed by Wood and Samson (2006), at standard state (25 °C and 1 bar), fluoride complexes is the dominant species of indium in hydrothermal fluid rather than hydroxide complexes when fluoride activities is greater than 10^{-3} and pH = 5. Indium may migrate efficiently under acidic, F-rich, and elevated temperature–pressure conditions, such as greisenization (Wood and Samson, 2006; Broman et al., 2018; Ivashchenko, 2021).

Greisenization is an important process causing re-enrichment of indium, and has been extensively studied (Yu et al., 2010; Ivashchenko, 2021; Xu et al., 2021c). During greisenization, F-rich, acidic and low-salinity magmatic fluids interact with granitic rocks, which leads to the alteration of biotite (the main carrier of indium and tin) into muscovite, and chlorite (Breiter et al., 2019; Launay et al., 2019, 2021). In this process, tin and indium were leached out from primary biotite or

other Sn-In-bearing minerals, resulting in the re-enrichment of tin and indium in hydrothermal fluids, which is evidenced by mass balance calculations applied to greisens (Ivashchenko, 2021; Xu et al., 2021c). As greisenization continues, the pH of the fluids increases and the temperature decreases, and then, the complexes of tin and indium become unstable and precipitate from the fluids (Chen et al., 2018; Gaskov and Gushchina, 2020). Fluorine and chlorine, as important ligands, are the most active components during greisenization (Yu et al., 2010; Chen et al., 2018). In the Gejiu district, such element redistribution was recently reported by Xu et al. (2021c), indicating that metal redistribution caused by greisenization could play an important role in Sn-In mineralization.

Although indium and tin can migrate together in hydrothermal processes, indium tends to concentrate in sphalerite rather than cassiterite when it precipitates. Indium is a chalcophile element with an ionic radius of 0.94 Å for hexahedral coordination and 0.76 Å for tetrahedral coordination (Shannon, 1976). The metal elements in sphalerite have similar ion radii and oxidation states, such as Zn^{2+} (0.74 Å), Cu^{+} (0.74 Å), and Fe^{2+} (0.78 Å), which are similar to In^{3+} (0.76 Å) in tetrahedral coordination. However, tin is tetravalent in cassiterite (SnO_2) with an ionic radius of 0.83 Å in hexahedral coordination, which is quite different from In^{3+}. Therefore, large amounts of In^{3+} tend to accumulate in sphalerite with a tetrahedral structure (Wang et al., 2019).

6. Prospects for future research

Abundant indium resources and an increasing number of In-bearing deposits have been reported in recent years in China, bringing new challenges to classic indium mineralization theory. We suggest that the followings should be strengthened in future research.

6.1. Indium mineralization in Sn-poor deposits

Since the indium concentration is much higher in granite-related Sn-polymetallic deposits than in other types of deposits, Sn-In polymetallic deposits are ideal for studying indium mineralization. However, some deposits with conspicuous indium enrichment were recently shown to be Sn-poor, which challenge the theory of relationship between tin and indium (Liu, 2017). Apart from the Qibaoshan Cu-polymetallic deposit, indium enrichment was also found in Sn-poor deposits such as the Chitudian Pb-Zn-Ag deposit in Henan province, with an average indium grade of 81 ppm (the authors' unpublished data), and the Dabaoshan Mo-W-Cu-Pb-Zn polymetallic deposit in Guangdong Province (Wu et al., 2019). These findings suggest that indium and tin may decouple in some cases, and tin is not necessary for indium enrichment. Unfortunately, the coupling and decoupling mechanisms of Sn-In are still unclear. Further investigations should give more focus on these Sn-poor deposits, which is significant for the recovery and reprocessing of indium from Sn-poor deposits.

6.2. Geochemical behavior of indium in melts and fluids

Although an intimate relationship between indium and tin has been observed in ores, rocks, and fluid inclusions, no experiments were conducted to demonstrate the effect of tin on indium enrichment. It is ambiguous whether tin and indium can form a certain complex compound in hydrothermal fluids, as proposed by Zhang et al. (2007). Therefore, understanding the behavior of indium during melt and fluid evolution and subsequent deportment in ore assemblages is fundamental to confine the metallogenic process of indium.

6.3. Pre-enrichment of indium

For In-bearing ores, the minimum grade for industrial operation is 5–10 ppm (Tu, 2004), which is approximately 100–200 times higher than the abundance of indium in continental crust (0.056 ppm). Because of the high concentration of indium in granitic hydrothermal systems, indium is considered to originate from granitic magma (Bauer et al., 2019). Therefore, the best candidate for indium mineralization is In-rich magma. Worldwide, Sn(-In) metallogenic belts are mainly distributed along the margins of ancient continents that separated from the Gondwana supercontinent (Romer and Kroner, 2016). Romer and Kroner (2014) suggested that the Gondwana supercontinent experienced strong chemical weathering during the Precambrian. As discussed in Section 2.2, tin and indium tend to be enriched in clay-rich sedimentary rocks produced by chemical weathering, and such rocks are ideal for generating Sn-In-rich magma by partial melting. Thus, chemical weathering may be an important control on the pre-enrichment of indium and tin. From this perspective, the relationship between indium and tin can be reasonably explained. Future studies should focus on the behavior of indium and tin during chemical weathering, which could provide new insight into the relationship between tin and indium.

6.4. Indium resources in silicate minerals

The occurrence state of indium in sphalerite has been well investigated (Section 3). Various methods, including leaching, electrolysis and flotation, have been widely applied to extract indium from different In-bearing raw materials (such as Zn concentrates, smelting slag, and dust), and the recovery rate of these methods is better than 95% (Du et al., 2017; Wang et al., 2017). However, andradites were recently proven to be an important In-bearing silicate mineral in the Dulong deposit, and the positive correlation between indium and iron suggests that In^{3+} may be incorporated into garnet by substituting Fe^{3+} (Xu et al., 2021b; Lyu et al., 2020). Because garnet is widespread in skarn-type deposits, it may host considerable indium resources. Unfortunately, we know little about the occurrence state of indium in silicate minerals, which results in wasted indium. In the future, more attention should be given to the occurrence state of indium in silicate minerals.

7. Conclusions

(1) Indium deposits in China are mainly associated with Sn-polymetallic deposits in the southwestern Yangtze Block, southern Great Xing'an Range, western Nanling Range, and their surrounding regions. Most of these indium deposits are related to Mesozoic granitic systems and the mineralization ages cluster at 70–100 Ma and 150–160 Ma.

(2) Sphalerite is the main carrier of indium, which is incorporated into the sphalerite crystal structure by a coupled substitution of $In^{3+} + Cu^{+}/Ag^{+} \leftrightarrow 2Zn^{2+}$. The relatively high availability of copper (and silver, to a lesser extent) in the mineralization system enable indium to enter sphalerite crystal lattice in large quantities.

(3) Indium is incompatible during partial melting and is compatible in biotite and amphibole during crystallization. It is transported in hydrothermal fluid as chloride complexes. The greisenization induced by F-rich magmatic fluid may play an important role in the enrichments of tin and indium. A strong correlation between indium and tin in granite-related magmatic-hydrothermal system suggests that the enrichments of tin and indium are controlled by the same physicochemical conditions.

(4) Tin and indium are minimally soluble during chemical weathering and could be adsorbed by clay minerals, which results in the pre-enrichment of Sn-In in sediments. Melting of such sedimentary rocks is ideal for generating Sn-In-rich magma and associated Sn-In mineralization.

(5) The discovery of Sn-poor deposits with indium enrichment suggest that tin and indium can decouple in some case. It is necessary to examine the geochemical behavior of indium in melts and hydrothermal fluids, which could contribute to a better

understanding of the coupling and decoupling mechanism of tin and indium.

Declaration of Competing Interest

The authors declare that they have no known competing financial interests or personal relationships that could have appeared to influence the work reported in this paper.

Acknowledgments

The authors are grateful to Dr. Austin Gion and an anonymous reviewer for their detailed and insightful comments that greatly improved the quality of our manuscript. We sincerely appreciate Associate Professor Alexandra Yang Yang for her helpful suggestions and language improvement on drafts of the manuscript. This work was supported by the National Natural Science Foundation of China (Nos. 92062102 & 41872088) and Applied Basic Research Foundation of Yunnan Province (Grant No. 202101AT070011).

Appendix A. Supplementary data

Supplementary data to this article can be found online at https://doi.org/10.1016/j.oregeorev.2022.104932.

References

Andersen, J.C.Ø., Stickland, R.J., Rollinson, G.K., Shail, R.K., 2016. Indium mineralisation in SW England: host parageneses and mineralogical relations. Ore Geol. Rev. 78, 213–238.

Audetat, A., Zhang, D., 2019. Abundances of S, Ga, Ge, Cd, In, Tl and 32 other major to trace elements in high-temperature (350–700 degrees °C) magmatic-hydrothermal fluids. Ore Geol. Rev. 109, 630–642.

Bauer, M.E., Burisch, M., Ostendorf, J., Krause, J., Frenzel, M., Seifert, T., Gutzmer, J., 2019. Trace element geochemistry of sphalerite in contrasting hydrothermal fluid systems of the Freiberg district, Germany: insights from LA-ICP-MS analysis, near-infrared light microthermometry of sphalerite-hosted fluid inclusions, and sulfur isotope geochemistry. Miner. Deposita 54, 237–262.

Breiter, K., Hložková, M., Korbelová, Z., Galiová, M.V., 2019. Diversity of lithium mica compositions in mineralized granite–greisen system: Cínovec Li-Sn-W deposit, Erzgebirge. Ore Geol. Rev. 106, 12–27.

Broman, C., Sundblad, K., Valkama, M., Villar, A., 2018. Deposition conditions for the indium-bearing polymetallic quartz veins at Sarvlaxviken, south-eastern Finland. Mineral Mag. 82, S43–S59.

Chen, Y.F., Wang, Y.W., Wang, J.B., Wang, L.J., Tang, P.Z., Shi, Y., Zhao, L.T., 2018. Greisenized alteration-mineralization geochemistry of the tin deposit related to A-type granite: case study on the Kamusite and Ganliangzi Deposits, Xinjiang. Earth Sci. 43, 3154–3168 in Chinese with English abstract.

Cheng, Y.B., Mao, J.W., 2010. Age and geochemistry of granites in Gejiu area, Yunnan province, SW China Constraints on their petrogenesis and tectonic setting. Lithos 120, 258–276.

Cheng, Y.B., Mao, J.W., Spandler, C., 2013. Petrogenesis and geodynamic implications of the Gejiu igneous complex in the western Cathaysia block, South China. Lithos 175, 213–229.

Cheng, Y.B., Mao, J.W., Rusk, B., Yang, Z.X., 2012. Geology and genesis of Kafang Cu-Sn deposit, Gejiu district, SW China. Ore Geol. Rev. 48, 180–196.

Clark, C., Fitzsimons, I.C., Healy, D., Harley, S.L., 2011. How does the continental crust get really hot? Elements 7, 235–240.

Cook, N.J., Ciobanu, C.L., Brugger, J., Etschmann, B., Howard, D.L., De Jonge, M.D., Ryan, C., Paterson, D., 2012. Determination of the oxidation state of Cu in substituted Cu-In-Fe-bearing sphalerite via -XANES spectroscopy. Am. Miner. 97, 476–479.

Cook, N.J., Ciobanu, C.L., Pring, A., Skinner, W., Shimizu, M., Danyushevsky, L., Saini-Eidukat, B., Melcher, F., 2009. Trace and minor elements in sphalerite: a LA-ICPMS study. Geochim. Cosmochim. Acta 73, 4761–4791.

Cook, N.J., Sundblad, K., Valkama, M., Nygård, R., Ciobanu, C.L., Danyushevsky, L., 2011. Indium mineralisation in A-type granites in southeastern Finland: insights into mineralogy and partitioning between coexisting minerals. Chem. Geol. 284, 62–73.

Dai, T.G., Du, G.F., Zhang, D.X., Wang, M.Y., 2012. Indium distribution in Dachang tin-polymetallic deposit of Guangxi Province. Chin. J. Nonferrous Met. 22, 703–714 in Chinese with English abstract.

Deng, J., Wang, Q.F., Li, G.J., 2017. Tectonic evolution, superimposed orogeny, and composite metallogenic system in China. Gondwana Res. 50, 216–266.

Dill, H.G., Garrido, M.M., Melcher, F., Gomez, M.C., Weber, B., Luna, L.I., Bahr, A., 2013. Sulfidic and non-sulfidic indium mineralization of the epithermal Au–Cu–Zn–Pb–Ag deposit San Roque (Provincia Rio Negro, SE Argentina) — with special reference to the "indium window" in zinc sulfide. Ore Geol. Rev. 51, 103–128.

Ding, T., Ma, D.S., Lu, J.J., Zhang, R.Q., 2018. Magnetite as an indicator of mixed sources for W-Mo–Pb–Zn mineralization in the Huangshaping polymetallic deposit, southern Hunan Province, China. Ore Geol. Rev. 95, 65–78.

Du, Y.P., Xie, X., Tong, X., Bai, F., 2017. A review of extraction and enrichment technology for indium. Value Eng. 36, 217–220 in Chinese with English abstract.

Duan, Q.F., Gao, L., Zeng, J.K., Zhou, Y., Tang, Z.Y., Li, K., 2014. Rb-Sr dating of sphalerite from Shizishan Pb-Zn deposit in Huayuan ore concentration area, westerm Hunan, and its geological significance. Earth Sci.-J. China Univ. Geosci. 39, 977–999 in Chinese with English abstract.

European Commission, Critical Raw Materials. Available online: https://ec.europa.eu/growth/sectors/rawmaterials/specific-interest/critical_en (accessed on 1 April 2019).

Fan, D.L., Zhang, T., Ye, J., Pašava, J., Kribek, B., Dobes, P., Varrin, I., Zak, K., 2004. Geochemistry and origin of tin–polymetallic sulfide deposits hosted by the Devonian black shale series near Dachang, Guangxi, China. Ore Geol. Rev. 24, 103–120.

Finger, F., Schiller, D., 2012. Lead contents of S-type granites and their petrogenetic significance. Contrib. Miner. Petrol. 164, 747–755.

Frenzel, M., Hirsch, T., Gutzmer, J., 2016. Gallium, germanium, indium, and other trace and minor elements in sphalerite as a function of deposit type — A meta-analysis. Ore Geol. Rev. 76, 52–78.

Gaskov, I.V., Gushchina, L.V., 2020. Physicochemical conditions of the formation of elevated indium contents in the ores of tin – sulfide and base-metal deposits in Siberia and far east: evidence from thermodynamic modeling. Geochem. Int. 58, 291–307.

Gion, A.M., Piccoli, P.M., Candela, P.A., 2018. Partitioning of indium between ferromagnesian minerals and a silicate melt. Chem. Geol. 500, 30–45.

Gion, A.M., Piccoli, P.M., Candela, P.A., 2019. Constraints on the formation of granite-related indium deposits. Econ. Geol. 114, 993–1003.

Guo, J., 2019. Tin mineralization events and fertility of granitoids in theYoujiang Basin, South China: The Gejiu and Dachang Sn-polymetalic districts as examples. Guangzhou Institute of Geochemistry, Chinese Academy of Sciences (in Chinese with English abstract), Guangzhou, China Ph.D. thesis.

Guo, C.L., Wang, D.H., Fu, X.F., Zhao, Z.G., Fu, D.M., Chen, Y.C., 2006. Discovery of in-rich ores in chahe tin deposits, Huili, Sichuan, and its significances. Geol. Rev. 52, 550–555 in Chinese with English abstract.

Guo, C.L., Wang, R.C., Yuan, S.D., Wu, S.H., Yin, B., 2015. Geochronological and geochemical constraints on the petrogenesis and geodynamic setting of the Qianlishan granitic pluton, Southeast China. Mineral. Petrol. 109, 253–282.

Guo, J., Zhang, R.Q., Li, C.Y., Sun, W.D., Hu, Y.B., Kang, D.M., Wu, J.D., 2018a. Genesis of the gaosong Sn-Cu deposit, Gejiu district, SW China: constraints from in situ LA-ICP-MS cassiterite U-Pb dating and trace element fingerprinting. Ore Geol. Rev. 92, 627–642.

Guo, J., Zhang, R.Q., Sun, W.D., Ling, M.X., Hu, Y.B., Wu, K., Luo, M., Zhang, L.C., 2018b. Genesis of tin-dominant polymetallic deposits in the Dachang district, South China: insights from cassiterite U-Pb ages and trace element compositions. Ore Geol. Rev. 95, 863–879.

Guo, Z.J., Song, Y.T., Xu, R.T., Wang, C.W., Yang, F., Wang, Q.L., Han, W., Liu, H.H., Kong, M., 2020. Characteristics of distribution and enrichment of indium in Gejiu tin polymetallic ore-concentrated area in Yunnan Province. Geoscience 34, 908–916 in Chinese with English abstract.

Hu, J.L., Chen, J.X., Xu, D.M., Wu, C.X., Zhang, K., Liu, J.S., Liu, A.X., Liu, C.P., 2017. Age and sources of the ore-forming material forthe Qibaoshan Cu-polymetallic deposit in Hu'nan Province: evidence from quartz vein Rb-Sr isotopic dating and S-Pb isotopes. Geol. Bull. China 36, 857–866 in Chinese with English abstract.

Hu, J.L., Xu, D.M., Zhang, K., Liu, J.S., 2016. Zircon U-Pb dating, Hf isotope and REE geochemistry of the quartz-porphyry in the Qibaoshan Cu-polymetallic deposit in Hunan. Geotect. Metal. 40, 1185–1199 in Chinese with English abstract.

Hu, R.Z., Wen, H.J., Ye, L., Chen, W., Xia, Y., Fan, H.F., Huang, Y., Zhu, J.J., Fu, S.L., 2020. Metallogeny of critical metals in the Southwestern Yangtze Block. Chin. Sci. Bull. 65, 3700–3714 in Chinese with English abstract.

Hu, X.Y., Bi, X.W., Shang, L.B., Hu, R.Z., Cai, G.S., Chen, Y.W., 2009. An experimental study of tin partition between melt and aqueous fluid in F/Cl-coexisting magma. Sci. Bull. 54, 1087–1097.

Huang, W.T., Lianga, H.Y., Zhang, J., Wu, J., Chen, X.L., Ren, L., 2019. Genesis of the Dachang Sn-polymetallic and Baoshan Cu ore deposits, and formation of a Cretaceous Sn-Cu ore belt from southwest China to western Myanmar. Ore Geol. Rev. 112, 103030.

Ishihara, S., Hoshino, K., Murakami, H., Endo, Y., 2006. Resource evaluation and some genetic aspects of indium in the Japanese ore deposits. Resour. Geol. 56, 347–364.

Ishihara, S., Murakami, H., Li, X., 2011a. Indium concentration in zinc ores in plutonic and volcanic environments: examples at the Dulong and Dachang mines, South China. Bull. Geol. Surv. Japan 7 (8), 259–272.

Ishihara, S., Murakami, H., Marquez-Zavalia, M.F., 2011b. Inferred indium resources of the Bolivian tin-polymetallic deposits. Resour. Geol. 61, 174–191.

Ishihara, S., Qin, K., Wang, Y., 2008. Resource evaluation of indium in the dajing tin-polymetallic deposits, Inner Mongolia, China. Resour. Geol. 58, 72–79.

Ivashchenko, V.I., 2021. Rare-metal (In, Bi, Te, Se, Be) mineralization of Skarn Ores in the Pitkäranta Mining District, Ladoga Karelia, Russia. Minerals 11, 124.

Jiang, S.H., Liang, Q.L., Liu, Y.F., Liu, Y., 2012. Zircon U-Pb ages of the magmatic rocks occurring in and around the Dajing Cu-Ag-Sn polymetallic deposit of Inner Mongolia and constrains to the ore-forming age. Acta Petrol. Sin. 28, 495–513 in Chinese with English abstract.

Jiang, S.Y., Zhao, K.D., Jiang, H., Su, H.M., Xiong, S.F., Xiong, Y.Q., Xu, Y.M., Zhang, W., Zhu, L.W., 2020. Spatiotemporal distribution, geological characteristics and metallogenic mechanism of tungsten and tin deposits in China: an overview. Chin. Sci. Bull 65, 3730–3745 in Chinese with English abstract.

Jovic, S.M., Guido, D.M., Schalamuk, I.B., Ríos, F.J., Tassinari, C.C.G., Recio, C., 2011. Pingüino In-bearing polymetallic vein deposit, Deseado Massif, Patagonia, Argentina: characteristics of mineralization and ore-forming fluids. Miner. Deposita 46, 257–271.

Keppler, H., Wyllie, P.J., 1991. Partitioning of Cu, Sn, Mo, W, U, and Th between melt and aqueous fluid in the systems haplogranite-H_2O-HCl and haplogranite-H_2O-HF. Contrib. Mineral. Petrol. 109, 139–150.

Krause, J., Reddy, S.M., Rickard, W.D. A., Saxey, D.W., Fougerouse, D., Bauer, M.E., 2020. Nanoscale compositional segregation in complex In-bearing sulfides: results from atom probe tomography and transmission kikuchi diffraction, EGU General Assembly 2020, Online, 4–8 May 2020, EGU2020-3473, https://doi.org/10.5194/egusphere-egu2020-3473.

Lai, S.H., 2014. Research on mineralization of the xianghualing tin polymetallic deposit, Hunan Province, China. M.Sc. thesis, Beijing, China University of Geosciences (in Chinese with English abstract).

Launay, G., Sizaret, S., Guillou-Frottier, L., Fauguerolles, C., Champallier, R., Gloaguen, E., 2019. Dynamic permeability related to greisenization reactions in Sn-W ore deposits: quantitative petrophysical and experimental evidence. Geofluids 2019, 1–23.

Launay, G., Sizaret, S., Lach, P., Melleton, J., Gloaguen, E., Poujol, M., 2021. Genetic relationship between greisenization and Sn–W mineralization in vein and greisen deposits: insights from the Panasqueira deposit (Portugal). BSGF - Earth Sci. Bull. 192, 2.

Li, H., Wu, J.H., Evans, N.J., Jiang, W.C., Zhou, Z.K., 2018. Zircon geochronology and geochemistry of the Xianghualing A-type granitic rocks: insights into multi-stage Sn-polymetallic mineralization in South China. Lithos 312, 1–20.

Li, T.J., Zhou, L., Zhao, Y.K., Zhu, G.S., Li, H.L., 2016. History and present situation of mineral resources exploitation and utilization in Dulong mine. Acta Mineral. Sin. 36, 463–470 in Chinese with English abstract.

Li, X.F., Yang, F., Chen, Z.Y., Bu, G.J., Wang, Y.T., 2010. A tentative discussion on geochemistry and genesis of indium in Dachang tin ore district, Guangxi. Miner. Depos. 29, 903–914 in Chinese with English abstract.

Li, X.F., Xu, J., Zhu, Y.T., Lv, Y.H., 2019. Critical minerals of indium: major ore types and scientific issues. Acta Petrol. Sin. 35, 3292–3302 in Chinese with English abstract.

Li, X.F., Zhu, Y.T., Xu, J., 2020. Indium as a critical mineral: a research progress report. Chin. Sci. Bull. 65, 3678–3687 in Chinese with English abstract.

Li, Y.B., Tao, Y., Zhu, F.L., Liao, M.Y., Xiong, F., Deng, X.Z., 2015. Distribution and existing state of indium in the Gejiu Tin polymetallic deposit, Yunnan Province, SW China. Chin. J. Geochem. 34, 469–483.

Liao, Y., Zhao, B., Zhang, D., Danyushevsky, L.V., Li, T., Wu, M., Liu, F., 2021. Evidence for temporal relationship between the late Mesozoic multistage Qianlishan granite complex and the Shizhuyuan W-Sn-Mo-Bi deposit. SE China. Sci. Rep. 11, 5828.

Liao, Z., Wang, Y.W., Wang, J.B., Li, H.M., Long, L.L., 2014. LA-ICP-MS cassiterite U-Pb dating of Dajimg tin-polymetallic deposit, Inner Mongolia, China. Miner. Depos. 33, 421–422 in Chinese.

Liu, J.J., Liu, J.M., Zheng, M.H., Zhou, Y.F., Gu, X.X., 1998. Indium enrichment in Cambrian gold deposits and its significance in Western Qinling Mountains. China. Gold Sci. Technol. 6, 25–26 in Chinese with English abstract.

Liu, J.P., 2017. Indium mineralization in a Sn-poor Skarn Deposit: a case study of the Qibaoshan Deposit, South China. Minerals 7, 76.

Liu, J.P., Gu, X.P., Shao, Y.J., Feng, Y.Z., Lai, J.Q., 2016. Indium mineralization in copper-tin stratiform skarn ores at the Saishitang-Rilonggou ore field, Qinghai, northwest China. Resour. Geol. 66, 351–367.

Liu, J.P., Rong, Y.N., Gu, X.P., Shao, Y.J., Lai, J.Q., Chen, W.K., 2018. Indium mineralization in the Yejiwei Sn-polymetallic deposit of the Shizhuyuan Orefield, Southern Hunan, China. Resour. Geol. 68, 22–36.

Liu, J.P., Rong, Y.N., Zhang, S.G., Liu, Z.F., Chen, W.K., 2017. Indium mineralization in the Xianghualing Sn-polymetallic orefield in Southern Hunan, Southern China. Minerals 7, 173.

Liu, M.T., Chen, X.P., Wang, J.S., Cao, J.Y., Niu, Y.J., Cheng, X.H., Zuo, L.B., 2019. Study on fluid inclusions and the mineralization of Dajing copper polymetallic deposit in Inner Mongolia. Geol. Surv. Res. 42, 194–201 in Chinese with English abstract.

Liu, S.Y., Liu, Y.P., Ye, L., Wang, D.P., 2021a. LA-ICPMS trace elements of pyrite from the super-large Dulong Sn-Zn polymetallic deposit, southeastern Yunnan, China. Acta Petrol. Sin. 37, 1196–1212 in Chinese with English abstract.

Liu, S.Y., Liu, Y.P., Ye, L., Wei, C., Cai, Y., Chen, W.H., 2021b. Genesis of Dulong Sn-Zn-In polymetallic deposit in Yunnan Province, South China: insights from Cassiterite U-Pb ages and trace element compositions. Minerals 11, 199.

Liu, Y.J., Cao, L.M., Li, Z.J., Wang, H.N., Chu, T.Q., Li, J.R., 1984. Element Geochemistry. Science Press, Beijing, 387–393 (in Chinese).

Liu, Y.P., Li, Z.X., Li, H.M., Guo, L.G., Xu, W., Ye, L., Li, C.Y., Pi, D.H., 2007. U-Pb geochronology of casiterite and zircon from the Dulong Sn-Zn deposit: evidence for Cretaceous large-scale granitic magmatism and mineralization even in southeasternYunnan province, China. Acta Petrol. Sin. 23, 967–976 in Chinese withEnglish abstract.

Lyu, Y.H., Li, X.F., Xu, J., 2020. Skarn mineralogy and mineral chemistry characteristics of Dulong Sn-Zn polymetallic deposit in Yunnan, China and their geological significances. J. Earth Sci. Environ. 42, 490–509 in Chinese with English abstract.

London, D., 1997. Estimating abundances of volatile and other mobile components in evolved silicic melts through mineral–melt equilibria. J. Petrol. 38, 1691–1706.

Lopez, L., Jovic, S.M., Guido, D.M., Permuy Vidal, C., Páez, G.N., Ruiz, R., 2015. Geochemical distribution and supergene behavior of indium at the Pingüino epithermal polymetallic vein system, Patagonia, Argentina. Ore Geol. Rev. 64, 747–755.

Mao, G.W., Zhu, Y.L., Hu, M.A., 2013. Geological characteristics and enrichment regularities of the dispersed elements indium and cadmium in the Zhongjia iron ore deposit of Longyan city, Fujian Province. Geol. Explor. 49, 130–143 in Chinese with English abstract.

Mao, J.W., Liu, P., Goldfarb, R.J., Goryachev, N.A., Pirajno, F., Zheng, W., Zhou, M.F., Zhao, C., Xie, G.Q., Yuan, S.D., Liu, M., 2021. Cretaceous large–scale metal accumulation triggered by post–subductional large–scale extension, East Asia. Ore Geol. Rev. 136, 104270.

Mao, J.W., Ouyang, H.G., Song, S.W., Santosh, M., Yuan, S.D., Zhou, Z.H., Zheng, W., Li, H., Liu, P., Cheng, Y.B., Chen, M.H., 2019a. Geology and metallogeny of tungsten and tin deposits in China. Soc. Econ. Geol. Special Publ. 22, 411–482.

Mao, J.W., Xie, G.Q., Yuan, S.D., Liu, P., Meng, X.Y., Zhou, Z.H., Zheng, W., 2018. Current research progress and future trends of porphyry skarn copper and granite related tin polymetallic deposits in the Circum Pacific metallogenic belts. Acta Petrol. Sin. (English Edition) 34, 2501–2517.

Mao, J.W., Yuan, S.D., Xie, G.Q., Song, S.W., Zhou, Q., Gao, Y.B., Liu, X., Fu, X.F., Gao, J., Zheng, Z.L., Li, T.G., Fan, X.Y., 2019b. New advances on metallogenic studies and exploration on critical minerals of China in 21st century. Miner. Deposi. 38, 689–698 in Chinese with English abstract.

Moura, M.A., Botelho, N.F., Olivo, G.R., Kyser, K., Pontes, R.M., 2014. Genesis of the Proterozoic Mangabeira tin-indium mineralization, Central Brazil: evidence from geology, petrology, fluid inclusion and stable isotope data. Ore Geol. Rev. 60, 36–49.

Murakami, H., Ishihara, S., 2013. Trace elements of Indium-bearing sphalerite from tin-polymetallic deposits in Bolivia, China and Japan: a femto-second LA-ICPMS study. Ore Geol. Rev. 53, 223–243.

Ni, P., Wang, G., Li, W., Chi, Z., Li, S., Gao, Y., 2021. A review of the Yanshanian ore-related felsic magmatism and tectonic settings in the Nanling W-Sn and Wuyi Au-Cu metallogenic belts, Cathaysia Block, South China. Ore Geol. Rev. 133, 104088.

Niu, H.B., Sun, W.D., Zhang, B.H., Chen, M.H., Zhang, B., Lu, S.L., 2020. Mineral chemistry of magnetite and its constraints on ore-forming processes of the Dulong Sn-Zn-n polymetallic deposit, southeastern Yunnan Province. Acta Petrol. Sin. 36, 154–170 in Chinese with English abstract.

Pavlova, G.G., Palessky, S.V., Borisenko, A.S., Vladimirov, A.G., Seifert, T., Phan, L.A., 2015. Indium in cassiterite and ores of tin deposits. Ore Geol. Rev. 66, 99–113.

Pearson, R.G., 1963. Hard and soft acids and bases. J. Am. Chem. Society 85, 3533–3539.

Pi, Q.H., Hu, R.Z., Wang, D.H., Miao, B.K., Qin, X.F., Chen, H.Y., 2015. Enrichment of indium in west ore belt of Dachang orefield: evidence from ore textures and sphalerite geochemistry. Miner. Depos. 34, 379–396 in Chinese with English abstract.

Pi, Q.J., Lu, D., Yang, X., Yu, H., 2019. The occurrence and enrichment of scattered indium: a case study of Dachang ore field in Guangxi, China. Earth Sci. 8, 303–316.

Romer, R.L., Kroner, U., 2014. Sediment and weathering control on the distribution of Paleozoic magmatic tin–tungsten mineralization. Miner. Deposita 50, 327–338.

Romer, R.L., Kroner, U., 2016. Phanerozoic tin and tungsten mineralization—Tectonic controls on the distribution of enriched protoliths and heat sources for crustal melting. Gondwana Res. 31, 60–95.

Rudnick, R.L., Gao, S., 2014. Composition of the continental crust. In: Holland, H.D., Turekian, K.K. (Eds.), Treatise on Geochemistry, Second Edition. Elsevier, Oxford, pp. 1–51.

Schulz, K.J., DeYoung, J.H., J., Seal, R.R., II., Bradley, D.C., 2017. Critical Mineral Resources of the United States—Economic and Environmental Geology and Prospects for Future Supply; U.S. Geological Survey Professional Paper; U.S. Geological Survey: Reston, VI, USA.

Schwarz-Schampera, U., 2014. Indium. In: Guns, G. (Ed.), Critical Metals Handbook. John Wiley & Sons, pp. 204–209.

Schwarz-Schampera, U., Herzig, P.M., 2002. Indium: Geology, Mineralogy, and Economics. Springer, Berlin, Heidelberg, pp. 1–216.

Seifert, T., Sandmann, D., 2006. Mineralogy and geochemistry of indium-bearing polymetallic vein-type deposits: implications for host minerals from the Freiberg district, Eastern Erzgebirge, Germany. Ore Geol. Rev. 28, 1–31.

Seward, T.M., Henderson, C., Charnock, J.M., 2000. Indium(III) chloride complexing and solvation in hydrothermal solutions to 350 degrees: an EXAFS study. Chem. Geol. 167, 117–127.

Shannon, R.D., 1976. Revised effective ionic radii and systematic study of inter atomic distances in halides and chalcogenides. Acta Cryst. 32, 751–767.

Shimizu, M., Kato, A., 1991. Roquesite-bearing tin ores from the Omodani, Akenobe, Fukoku, and Ikuno polymetallic vein-type deposits in the inner zone of southwestern Japan. Can. Mineral. 29, 207–215.

Shimizu, T., Morishita, Y., 2012. Petrography, chemistry, and near-infrared microthermometry of indium-bearing sphalerite from the Toyoha polymetallic deposit, Japan. Econ. Geol. 107, 723–735.

Simons, B., Andersen, J.C.Ø., Shail, R.K., Jenner, F.E., 2017. Fractionation of Li, Be, Ga, Nb, Ta, In, Sn, Sb, W and Bi in the peraluminous Early Permian Variscan granites of the Cornubian Batholith: precursor processes to magmatic-hydrothermal mineralisation. Lithos 278–281, 491–512.

Song, W.M., Gong, E.P., Liu, S.W., Fu, J.X., 2014. Study on the geochronology of Meng'entaolegai pluton in Horqin right wing middle banner, Inner Mongolia. J. Northeastern Univ. 35, 898–902 in Chinese with English abstract.

Sui, Q.L., Zhu, L.H., Sun, S.J., Chen, D.H., Zhao, X.J., Wang, Z.F., 2020. The geochemical behavior of tin and Late Cretaceous tin mineralization in South China. Acta Petrol. Sin. 36 (01), 23–34 in Chinese with English abstract.

Sun, S.S., 1982. Chemical-composition and origin of the Earth's primitive mantle. Geochim. Cosmochim. Acta 46, 179–192.

Sylvester, P.J., 1998. Post-collisional strongly peraluminous granites. Lithos 45, 29–44.

Torró, L., Melgarejo, J., Gemmrich, L., Mollinedo, D., Cazorla, M., Martínez, Á., Pujol-Solà, N., Farré-De-Pablo, J., Camprubí, A., Artiaga, D., Torres, B., Alfonso, P., Arce, O., 2019. Spatial and temporal controls on the distribution of indium in xenothermal vein-deposits: the Huari Huari district, Potosí, Bolivia. Minerals 9, 304.

Trofimov, N.D., Trigub, A.L., Tagirov, B.R., Filimonova, O.N., Evstigneeva, P.V., Chareev, D.A., Kvashnina, K.O., Nickolsky, M.S., 2020. The state of trace elements (In, Cu, Ag) in sphalerite studied by X-ray absorption spectroscopy of synthetic minerals. Minerals 10, 640.
Tu, G.C., 2004. The Geochemistry and Ore-Forming Mechanism of the Dispersed Elements. Geological Publishing House, Beijing, pp. 317–367 in Chinese.
USGS (United States Geological Survey), 2021. Mineral Commodity Summaries 2011-2021. https://www.usgs.gov/centers/nmic/indium-statistics-and-information.
Valkama, M., Sundblad, K., Cook, N.J., Ivashchenko, V.I., 2016a. Geochemistry and petrology of the indium-bearing polymetallic Skarn Ores at Pitkäranta, Ladoga Karelia, Russia. Miner. Deposita 51, 823–839.
Valkama, M., Sundblad, K., Nygård, R., Cook, N., 2016b. Mineralogy and geochemistry of indium-bearing polymetallic veins in the Sarvlaxviken area, Lovisa, Finland. Ore Geol. Rev. 75, 206–219.
Wang, D.P., Zhang, Q., Wu, L.Y., Ye, L., Liu, Y.P., Lan, J.B., 2019. The relationship between indium and tin, copper, lead and zinc in granite and its significance to indium mineralization. Acta Petrol. Sin. 35, 3317–3332 in Chinese with English abstract.
Wang, H., Feng, C.Y., Li, D.X., Li, C., Ding, T.Z., Liao, F.Z., 2016. Geology, geochronology and geochemistry of the Saishitang Cu deposit, East Kunlun Mountains, NW China: constraints on ore genesis and tectonic setting. Ore Geol. Rev. 72, 43–59.
Wang, H., Wen, S.M., Feng, Q.C., Wang, Y.J., Han, G., 2017. The development and prospects of indium enrichment and separation technology. Value Eng. 36, 51–54 in Chinese with English abstract.
Wang, J.S., Wen, H.J., Li, C., Ding, W., Zhang, J.R., 2011. Re-Os isotope dating of arsenopyrite from the quartz vein-type gold deposit, Southeastern Guizhou province, and its geological implications. Acta Geol. Sin. 85 (6), 955–964 in Chinese with English abstract.
Wang, L.J., Wang, J.B., Wang, Y.W., Long, L.L., 2015. Metallogenic mechanism of fluid and prospecting forecast of DajingSn-Cu polymetallic deposit, Inner Mongolia. Acta Petrol. Sin. 31, 991–1001 in Chinese with English abstract.
Wang, Q.F., Yang, L., Xu, X.J., Santosh, M., Wang, Y.N., Wang, T.Y., Chen, F.G., Wang, R. X., Gao, L., Liu, X.F., Yang, S.J., Chen, J.H., Zhang, Q.Z., Deng, J., 2020. Multi-stage tectonics and metallogeny associated with Phanerozoic evolution of the South China Block: a holistic perspective from the Youjiang Basin. Earth-Sci. Rev. 211, 103405.
Wang, S.H., He, S., Huang, H.X., 2014. Discovery of roquesite in the Zijinshan Cu- Au deposit, Fujian Province, and its implications for deep exploration. Geol. Bull. China 33, 1425–1429 in Chinese with English abstract.
Werner, T.T., Mudd, G.M., Jowitt, S.M., 2017. The world's by-product and critical metal resources part III: a global assessment of indium. Ore Geol. Rev. 86, 939–956.
Wolf, M., Romer, R.L., Franz, L., López-Moro, F.J., 2018. Tin in granitic melts: the role of melting temperature and protolith composition. Lithos 310–311, 20–30.
Wood, S.A., Samson, I.M., 2006. The aqueous geochemistry of gallium, germanium, indium and scandium. Ore Geol. Rev. 28, 57–102.
Wu, J.B., Pi, Q.H., Hu, Y.H., Wei, C.W., Li, G., Yang, X., 2019. Occurrence state of scattered elements in Dabaoshan polymetallic Deposits. J. Guilin Univ. Technol. 39, 537–550.
Wu, Y.T., 2009. Study on the Enrichment Regularity of Indium in Dachang Ore-field, Guangxi. Central South University (in Chinese with English abstract), Changsha, China. Ph.D. thesis.
Xiao, C., Shen, Y., Wei, C., 2019. Petrogenesis of Low Sr and high Yb A-type granitoids in the Xianghualing Sn polymetallic deposit, South China: constrains from geochronology and Sr-Nd-Pb-Hf isotopes. Minerals 9, 182.
Xu, B., Jiang, S.Y., Wang, R., Ma, L., Zhao, K.D., Yan, X., 2015. Late Cretaceous granites from the giant Dulong Sn-polymetallic ore district in Yunnan Province, South China: geochronology, geochemistry, mineral chemistry and Nd–Hf isotopic compositions. Lithos 218–219, 54–72.
Xu, J., Ciobanu, C.L., Cook, N.J., Slattery, A., Li, X.F., 2021a. Phase relationships in the system ZnS-CuInS: insights from a nanoscale study of indium-bearing sphalerite. Am. Miner. 106, 192–205.
Xu, J., Cook, N.J., Ciobanu, C.L., Li, X.F., Kontonikas-Charos, A., Gilbert, S., Lv, Y.H., 2021b. Indium distribution in sphalerite from sulfide–oxide–silicate skarn assemblages: a case study of the Dulong Zn–Sn–In deposit, Southwest China. Miner. Deposita 56, 207–324.
Xu, J., Li, X.F., 2018. Spatial and temporal distributions, metallogenic backgrounds and processes of indium deposits. Acta Petrol. Sin. 34, 3611–3626 in Chinese with English abstract.
Xu, R., Deng, J., Cheng, H.Y., Cui, X.L., Wang, C.B., 2018. Geochronology, geochemistry and geodynamic setting of Late Cretaceous magmatism and Sn mineralization in the western South China and Tengchong Baoshan. Acta Petrol. Sin. 34, 1271–1284 in Chinese with English abstract.
Xu, R., Romer, R.L., Glodny, J., 2021c. External fluids cause alteration and metal redistribution in the granite-hosted Tangziwa Sn Cu deposit, Gejiu district, China. Lithos 382–383, 105937.
Ye, L., Bao, T., Liu, Y.P., He, F., Wang, X.J., Zhang, Q., Wang, D.P., Lan, J.B., 2018. The trace and rare earth elements in scheelites and their implication for the mineralization in Dulong Sn-Zn polymetal ore deposit, Yunnan Province. J. Nanjing Univ. 54, 245–258 in Chinese with English abstract.
Ye, L., Cook, N.J., Ciobanu, C.L., Liu, Y.P., Zhang, Q., Liu, T.G., Gao, W., Yang, Y.L., Danyushevskiy, L., 2011. Trace and minor elements in sphalerite from base metal deposits in South China: a LA-ICPMS study. Ore Geol. Rev. 39, 188–217.
Ye, L., Liu, Y.P., Zhang, Q., Bao, T., He, F., Wang, X.J., Wang, D.P., Lan, J.B., 2017. Trace and rare earth elements characteristics of sphalerite in dulong super large Sn-Zn polymetallic ore deposit, Yunnan Province. J. Jilin Univ. 47, 734–750 in Chinese with English abstract.
Yu, A.P., Wang, R.C., Zhu, J.C., Xie, L., Zhang, W.L., Che, X.D., 2010. Mineralogical study on greisenization zoning and tin mineralization in Huashan granite, Guangxi, South China. Geol. J. China Univ. 16, 281–293 in Chinese with English abstract.
Yu, Z.X., 1997a. Damiaoite — a new native indium and platinum alloy. Acta Geol. Sin. 71, 328–331 in Chinese with English abstract.
Yu, Z.X., 1997b. Yixunite — an ordered new native indium and platinum alloy. Acta Geol. Sin. 71, 332–335 in Chinese with English abstract.
Yuan, S.D., Mao, J.W., Zhao, P.L., Yuan, Y.B., 2018. Geochronology and petrogenesis of the Qibaoshan Cu-polymetallic deposit, northeastern Hunan Province: implications for the metal source and metallogenic evolution of the intracontinental Qinhang Cu-polymetallic belt, South China. Lithos 302–303, 519–534.
Yuan, S.D., Peng, J.T., Shen, N.P., Hu, R.Z., Dai, T.M., 2007. ^{40}Ar-^{39}Ar isotopic dating of the Xianghualing Sn-polymetallic orefield in Southern Hunan, China and its geological implications. Acta Geol. Sin. (English Edition) 81, 278–286.
Yuan, S.D., Peng, J., Hu, R.Z., Li, H.M., Shen, N.P., Zhang, D.L., 2008. A precise U-Pb age on cassiterite from the Xianghualing tin-polymetallic deposit (Hunan, South China). Miner. Deposita 43, 375–382.
Yuan, S.D., Williams-Jones, A.E., Romer, R.L., Zhao, P.L., Mao, J.W., 2019. Protolith-related thermal controls on the decoupling of Sn and W in Sn-W metallogenic Provinces: insights from the Nanling Region, China. Econ. Geol. 114, 1005–1012.
Yuan, Y., Xue, F., Li, S.T., Liu, Y.L., 2020. The distribution regularity of rare metal indium and preliminary estimation of metal resources in the lead-zinc deposits in China. Miner. Resour. Geol. 34, 203–209 in Chinese with English abstract.
Zhang, J.F., Pang, Q.B., Zhu, Q., Jin, C.Z., 2003a. Mengentaolegai Ag-Pb-Zn deposit in Inner Mongolia: Ar Ar age of muscovite and its significance. Miner. Depos. 22, 253–256.
Zhang, K.J., 2017. A Mediterranean-style model for early Neoproterozoic amalgamation of South China. J. Geodyn. 105, 1–10.
Zhang, L.P., Zhang, R., Hu, Y.B., Liang, J.L., Ouyang, Z.X., He, J.J., Chen, Y.X., Guo, J., Sun, W.D., 2017. The formation of the Late Cretaceous Xishan Sn–W deposit, South China: geochronological and geochemical perspectives. Lithos 290, 253–286.
Zhang, L.P., Zhang, R.Q., Wu, K., Chen, Y.X., Li, C.Y., Hu, Y.B., He, J.J., Liang, J.L., Sun, W.D., 2018a. Late Cretaceous granitic magmatism and mineralization in the Yingwuling W– Sn deposit, South China: constraints from zircon and cassiterite U-Pb geochronology and whole-rock geochemistry. Ore Geol. Rev. 96, 115–129.
Zhang, Q., 1987. Trace elements in galena and sphalerite and their geochemical significance in distinguishing the genetic types of Pb-Zn ore deposits. Chin. J. Geochem. 6, 177–190.
Zhang, Q., Liu, Z.H., Zhan, X.Z., Shao, S.X., 2003b. Specialization of ore deposit types and minerals for enrichment of indium. Miner. Depos. 22, 309–316 in Chinese with English abstract.
Zhang, Q., Liu, Z.H., Zhan, X.Z., Shao, S.X., 2004. Trace element geochemistry of Meng'entaolegai Ag-Pb-Zn-in deposit, Inner Mongolia, China. Acta Mineral. Sin. 24, 39–47 in Chinese with English abstract.
Zhang, Q., Zhan, X.Z., Pan, J.Y., Shao, S.X., 1998. Geochemical enrichment and mineralization of indium. Chin. J. Geochem. 17, 221–225.
Zhang, Q., Zhan, X.Z., Qiu, Y.Z., Shao, S.X., Liu, Z.H., 2002. Lead isotopic composition and lead source of the Meng'entaolegai Ag-Pb-Zn-In deposit in Inner Mongolia. Geochimica 31, 253–258 in Chinese with English abstract.
Zhang, Q., Zhu, X.Q., He, Y.L., Jiang, J.J., Wang, D.P., 2006. Indium enrichment in the Meng'entaolegai Ag-Pb-Zn deposit, Inner Mongolia, China. Resour. Geol. 56, 337–346.
Zhang, Q., Zhu, X.Q., He, Y.L., Zhu, Z.H., 2007. In, Sn, Pb and Zn contents and their relationships in ore-forming fluids from some In-rich and in-poor deposits in China. Acta Geol. Sin. (English Edition) 81, 450–462.
Zhang, Y., Gao, J.F., Ma, D.S., Pan, J.Y., 2018b. The role of hydrothermal alteration in tungsten mineralization at the Dahutang tungsten deposit, South China. Ore Geol. Rev. 95, 1008–1027.
Zhao, K., Zhang, L., Palmer, M.R., Jiang, S., Xu, C., Zhao, H., Chen, W., 2021. Chemical and boron isotopic compositions of tourmaline at the Dachang Sn-polymetallic ore district in South China: constraints on the origin and evolution of hydrothermal fluids. Miner. Deposita 56, 1589–1608.
Zhao, P.L., Chu, X., Williams-Jones, A.E., Mao, J.W., Yuan, S.D., 2022a. The role of phyllosilicate partial melting in segregating tungsten and tin deposits in W-Sn metallogenic provinces. Geology 50, 121–125.
Zhao, P.L., Yuan, S.D., Mao, J.W., Yuan, Y.B., Zhao, H.J., Zhang, D.L., Shuang, Y., 2018a. Constraints on the timing and genetic link of the large-scale accumulation of proximal W-Sn–Mo–Bi and distal Pb–Zn–Ag mineralization of the world-class Dongpo orefield, Nanling Range, South China. Ore Geol. Rev. 95, 1140–1160.
Zhao, P.L., Yuan, S.D., Williams-Jones, A.E., Romer, R.L., Yan, C., Song, S.W., Mao, J.W., 2022b. Temporal separation of W and Sn mineralization by temperature-controlled incongruent melting of a single protolith: evidence from the Wangxianling Area, Nanling Region, South China. Econ. Geol. 117, 667–682.
Zhao, P.L., Zajacz, Z., Tsay, A., Yuan, S.D., 2022c. Magmatic-hydrothermal tin deposits form in response to efficient tin extraction upon magma degassing. Geochim. Cosmochim. Acta 316, 331–346.
Zhao, Y.Y., Liu, Y., Cui, Y.B., Lv, L.N., Song, L., Qu, X.M., 2010. Discovery and significance of indium mineralization belt in Bangong Lake—Nujiang River metallogenic belt and adjacent regions in Xizang (Tibet). Geol. Rev. 56, 568–578 in Chinese with English abstract.
Zeng, Q.D., Liu, J.M., Chu, S.X., Guo, Y.P., Gao, S., Guo, L.X., Zhai, Y.Y., 2016. Poly-metal mineralization and exploration potential in southern segment of the Da Hinggan mountains. J. Jilin Univ. 46, 1100–1123 in Chinese with English abstract.
Zhao, Z.Y., Hou, L., Ding, J., Zhang, Q.M., Wu, S.Y., 2018b. A genetic link between Late Cretaceous granitic magmatism and Sn mineralization in the southwestern South

China Block: a case study of the Dulong Sn-dominant polymetallic deposit. Ore Geol. Rev. 93, 268–289.
Zhou, Z., Wen, H., 2021. A magmatic-hydrothermal indium-bearing polymetallic vein mineralization belt in the western Jiangnan Orogen: evidence from zinc and cadmium isotopes of sphalerite. Ore Geol. Rev. 131, 103843.
Zhou, Z., Wen, H., Qin, C., Liu, L., 2017. Geochemical and isotopic evidence for a magmatic-hydrothermal origin of the polymetallic vein-type Zn-Pb deposits in the northwest margin of Jiangnan Orogen, South China. Ore Geol. Rev. 86, 673–691.
Zhu, X.Q., Zhang, Q., He, Y.L., Shao, S.X., 2004. Genesis of Meng'entaolegai Ag-Pb-Zn-In polymetallic deposit in Inner Mongolia. Miner. Depos. 23, 52–60 in Chinese with English abstract.
Zhu, X.Q., Zhang, Q., He, Y.L., Zhu, C.H., 2006. Relationships between indium and tin, zinc and lead in ore-forming fluid from the In-rich and -poor deposits in China. Geochimica 35, 6–12 in Chinese with English abstract.